IOSR Journal Of Applied Physics (IOSR-JAP)
e-ISSN: 2278-4861.Volume 16, Issue 2 Ser. 1 (Mar. – Apr. 2024), PP 50-71
www.Iosrjournals.Org

Vibrational Assignments, Structural and Molecular Properties of Acetaminophen and Diclofenac: Computational Evaluation using Density Functional Theory

Ravikantha M. N. [A,B], Vibha K [B], Prachalith N. C. [B], Annoji Reddy R. [B,C], Shilpa K. G.[D] Thipperudrappa J. [B,*]

[A] *Department Of Physics, Government Science College, Chitradurga - 577 501, Karnataka, India.*
[B] *Department Of Physics, Vijayanagara Sri Krishnadevaraya University, Ballari - 583 104, Karnataka, India.*
[C] *Department Of Physics, GVVP Government First Grade College, Hagari Bommana Halli – 583 212, Karnataka, India.*
[D] *Department Of Chemistry, Vijayanagara Sri Krishnadevaraya University, Ballari - 583 104, Karnataka, India.*

Abstract
The present work focuses on spectroscopic analysis of the Acetaminophen and Diclofenac combined with DFT investigations using hybrid functionals with 6-311++ G(d,p) basis set. The computed geometrical parameters and the scaled harmonic frequencies are in good agreement with experimental data.The vibrational assignments of normal modes were performed using VEDAsoftware. The Frontier Molecular Orbital (FMO)and Density of States (DOS)analysis was done to simulate HOMO-LUMO plots. The estimated gaps are found to be 5.24 eV and 4.95 eV (using B3LYP) for acetaminophen and diclofenac respectively. The study extended to compute the reactivity descriptors which show that diclofenac is more reactive and softer (lower band gap) than acetaminophen.The DOS and Partial DOS graphs were examined to unveil their electronic character. Molecular electrostatic potential (MEP) portraitsshow the strongest electronegative region around the C=O bonds which is the key feature of COX-inhibitors. The Natural Bond Orbital (NBO) scheme suggests that lone pair interactions LP(1)(N_{13})→π(C_{15}-O_{16}) in acetaminophen and LP(2)(O_{11})→π*(C_2-C_3) in diclofenac are responsible for molecular stability. The computed non-linear optical descriptors indicate that these molecules are promising materials for non-linear optical applications.The Atoms in molecule (AIM) and Non-covalent Interaction (NCI) analysis gave more insights into the nature of interactions. It was found that both attractive and repulsive interactions leads to the stabilization of the structure.*

Keywords:*Vibrational Assignments, NBO, FMO, PDOS, NLO, AIM, NCI.*

Date of Submission: 06-04-2024 Date of Acceptance: 16-04-2024

I. Introduction

Many experimental studies reported that the interaction of substituent groups on the ring system of organic bioactive molecules play an important role in exploring reactive sites responsible for their biological activity[1] and are of great interest to gain a deeper insight into the mode of probable action which helps in improving the drug efficacy. These interactions can be examined by the structural, vibrational, and other molecular properties[2].

Non-steroidal anti-inflammatory drugs (NSAIDs) are the most commonly used class of bioactive molecules with anti-inflammatory, pain reliever, and fever reduceractivity, which are important in the treatment of many diseases. The therapeutic effects of NSAIDs and their clinical importance in chronic pain was reported by Yuen Ho[3]. Acetaminophen (N4HPA) and Diclofenac (2DAPA) are bioactive moleculesbelonging to the class of NSAIDs, the former with very littleanti-inflammatory action, while the latter is known for its topical anti-inflammatory activity[4].

The mode of action and most of its other pharmacological effects of the NSAIDs are primarily accredited to the inhibition of conversion of arachidonic acid to prostaglandins (PGs), which are mediators of the inflammatory process[5]. As proposed by Vane, the C=O group of the N4HPA and 2DAPAmolecules plays a vital role in a efficacious specific interactions with the cyclooxygenase (COX) isoenzymes inhibiting the synthesis of prostaglandins in the human body[6].

Acetaminophen possesses strong analgesic and antipyreticproperties[7] and has relatively moderate side effects[8]. Reported data suggests that the nonopioid analgesic activity of N4HPA is due to its anti-cyclooxygenase properties[9]. Diclofenac is considered to be the best inhibitor of the cyclooxygenase (COX-2) enzyme among its class of drugs[10] with analgetic, anti-rheumatic, antipyretic properties, and potentially even extending to cancer therapy[11].

Many investigators reported the efficacy of Acetaminophen and Diclofenac in the treatment of various diseases. Malhotra et al., investigated the efficacy of analgesic, anti-pyretic and anti-inflammatory properties of Diclofenac, Acetaminophen and their combination in experimental animals[12]. Akhavanakbari et al studied effects of N4HPA and 2DAPA suppository on pain and opioids consumption after caesarean section[13].

Very often, quantum computational methods were used for the accurate prediction of a variety of molecular properties[14]. Owing to their significant applications, NSAIDs have also been the subject of quantum computational studies. To the best of our knowledge, the detailed literature review revealed that the analysis of reactivity of the proposed molecules using DFT functionals have not been invoked. This inadequacy in the literature encouraged us to take up the present work. The initial geometrical optimization and subsequent calculations and analysis were carried out by employing different hybrid DFT functionals.

II. Procedure

Sample

The experimental samples N4HPA and 2DAPA were procured from Sigma–Aldrich, India with a stated purity of 99% and used for experimentation without further purification. Chemical structure of N4HPA and 2DAPA are given below in the Fig1(a) and Fig1(b) respectively.

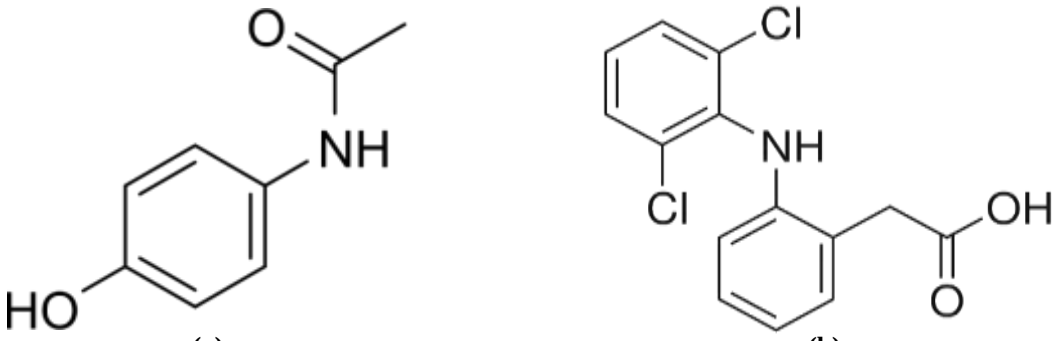

(a) **(b)**

Figure 1: Molecular structure of (a) Acetaminophen ($C_8H_9NO_2$) and (b) Diclofenac ($C_{14}H_{11}Cl_2NO_2$).

Instrumentation

The room temperature Fourier transform infrared (FT-IR) spectrum of the outlined molecules in the solid phase was recorded using KBr pellet technique on Perkin-Elmer FT-IR spectrometer, in the range 4000–400 cm^{-1} with a resolution of 0.5 cm^{-1}.

Computational Techniques

In the present work, a variety of molecular properties of the outlined molecules were explored computationally using DFT functionals; B3LYP, B3PW91, mPW1PW91and CAM-B3LYPwith Pople's the triple split valence basis set; 6-311++G(d,p).

The computations were done using Gaussian 09W:RevC.01 quantum computational package[15] andall the molecular simulationsof the Gaussian output were rendered by Gauss View 6.0.16[16].The theoretically generated vibrational spectrum is interpreted through the Potential Energy Distribution (PED) Matrix using VEDA4.1eprogram[17]. The quantitative analysis of MEP and FMO were carried out using multiwfn v3.7 program[18] and HOMO-LUMO energies and Global reactivity descriptorsare proposed. Further, the FMO information is convoluted for DOS analysis. NBO Population analysis was performed using NBO v3.1 program[19] embedded in Gaussian 09W to understand the interactions between the orbitals. Using the optimized coordinates, the first and second static hyperpolarizabilities were calculated by the finite field perturbation method in order to find the potentiality of title molecules as NLO candidates.Also, Gaussian output was convoluted through AIMAll Professional Ver.10.5.04 Package[20] to perform topological analysis of electron density at bond and ring critical points (BCP & RCP) based on QTAIM.

III. Results And Discussion

Geometrical optimization

The parent structure of the molecules for computation was acquired from GaussView GUI. For each structure, molecular geometry was fully optimized without symmetry constraints using Berny's optimization algorithm implemented in Gaussian package. The DFT results confirmed thatthe obtained structures represent global minimum on the potential energy hyper surfaces. The optimized molecular geometry with numeration scheme for atoms in the isolated molecule of N4HPA and 2DAPA are displayed in Fig 2.

(*a*) (*b*)

Figure 2: Ground state optimized geometry of (a) acetaminophen and (b) Diclofenac molecules with the numeration scheme for atoms.

Structural Parameters

The structural parameters (The bond lengths, bond angles and dihedral angles) on the optimized geometry for N4HPA and 2DAPA computed from DFT methods using 6311G++(d,p) basis set are presented in the Table 1 and 2 respectively, along with previously reported single crystal XRD parameters of similar geometry for comparison[21,22].

In order to investigate the performance of the DFT functionals, the MAE($\overline{\Delta y}$) between computed (y_i^{cal}) and optimal (y_i^{opt}) bond parameters[23] were estimated for all applied DFT methods using the expression: $MAE = (\overline{\Delta y}) = \frac{1}{N}\sum|y_i^{cal} - y_i^{opt}|$.

Table 1: Structural parameters (bond lengths in Å, and bond angles in degrees) of Acetaminophen.

Atomic Definition	Exp. #	Calculated with DFT/ 6-311++G(d,p)			
		B3LYP	B3PW91	mPW1PW91	CAM-B3LYP
Bond Lengths					
$r_1(C_1\text{-}C_2)$	1.3905	1.3950	1.3932	1.3912	1.3888
$r_2(C_1\text{-}C_6)$	1.3887	1.3872	1.3849	1.3831	1.3816
$r_3(C_1\text{-}H_7)$	0.9801	1.0830	1.0840	1.0826	1.0824
$r_4(C_2\text{-}C_3)$	1.3950	1.3930	1.3914	1.3892	1.3861
$r_5(C_2\text{-}O_{11})$	1.3708	1.3713	1.3646	1.3616	1.3658
$r_6(C_3\text{-}C_4)$	1.3839	1.3940	1.3914	1.3897	1.3893
$r_7(C_3\text{-}H_8)$	0.9699	1.0862	1.0872	1.0858	1.0854
$r_8(C_4\text{-}C_5)$	1.3941	1.3985	1.3962	1.3940	1.3913
$r_9(C_4\text{-}H_9)$	0.9747	1.0790	1.0805	1.0791	1.0784
$r_{10}(C_5\text{-}C_6)$	1.3974	1.4020	1.3997	1.3976	1.3955
$r_{11}(C_5\text{-}N_{13})$	1.4182	1.4158	1.4095	1.4076	1.4135
$r_{12}(C_6\text{-}H_{10})$	0.9440	1.0860	1.0870	1.0856	1.0853
$r_{13}(O_{11}\text{-}H_{12})$	0.9047	0.9627	0.9611	0.9588	0.9610
$r_{14}(N_{13}\text{-}H_{14})$	0.9274	1.0081	1.0075	1.0058	1.0068
$r_{15}(N_{13}\text{-}C_{15})$	1.3447	1.3750	1.3711	1.3680	1.3679
$r_{16}(C_{15}\text{-}O_{16})$	1.2376	1.2195	1.2174	1.2149	1.2143
$r_{17}(C_{15}\text{-}C_{17})$	1.5055	1.5201	1.5148	1.5120	1.5130
$r_{18}(C_{17}\text{-}H_{18})$	0.9493	1.0919	1.0923	1.0908	1.0904
$r_{19}(C_{17}\text{-}H_{19})$	0.9454	1.0919	1.0923	1.0908	1.0904
$r_{20}(C_{17}\text{-}H_{20})$	0.9809	1.0921	1.0924	1.0910	1.0906
MAE		**0.0105**	**0.0099**	**0.0091**	**0.0082**
Bond Angles					
$\alpha_1(C_2\text{-}C_1\text{-}C_6)$	120.074	119.770	119.815	119.809	119.721
$\alpha_2(C_2\text{-}C_1\text{-}H_7)$	119.114	119.329	119.301	119.280	119.248
$\alpha_3(C_6\text{-}C_1\text{-}H_7)$	120.812	120.902	120.884	120.911	121.031
$\alpha_4(C_1\text{-}C_2\text{-}C_3)$	119.381	119.415	119.295	119.297	119.477
$\alpha_5(C_1\text{-}C_2\text{-}O_{11})$	118.348	117.484	117.613	117.632	117.532

$\alpha_6(C_3\text{-}C_2\text{-}O_{11})$	122.270	123.101	123.092	123.070	122.991
$\alpha_7(C_2\text{-}C_3\text{-}C_4)$	120.379	120.977	121.047	121.057	120.945
$\alpha_8(C_2\text{-}C_3\text{-}H_8)$	119.908	120.004	119.994	119.976	119.980
$\alpha_{10}(C_3\text{-}C_4\text{-}C_5)$	120.195	119.790	119.808	119.787	119.751
$\alpha_{11}(C_3\text{-}C_4\text{-}H_9)$	120.899	120.526	120.617	120.619	120.564
$\alpha_{12}(C_5\text{-}C_4\text{-}H_9)$	119.180	119.684	119.575	119.594	119.685
$\alpha_{13}(C_4\text{-}C_5\text{-}C_6)$	118.905	118.863	118.821	118.837	118.935
$\alpha_{14}(C_4\text{-}C_5\text{-}N_{13})$	123.977	123.637	123.625	123.635	123.654
$\alpha_{15}(C_6\text{-}C_5\text{-}N_{13})$	116.821	117.501	117.554	117.528	117.411
$\alpha_{16}(C_1\text{-}C_6\text{-}C_5)$	120.414	121.185	121.214	121.213	121.171
$\alpha_{18}(C_5\text{-}C_6\text{-}H_{10})$	119.792	119.773	119.778	119.759	119.734
$\alpha_{19}(C_2\text{-}O_{11}\text{-}H_{12})$	111.323	109.720	109.442	109.508	109.987
$\alpha_{20}(C_5\text{-}N_{13}\text{-}H_{14})$	114.584	114.851	114.895	114.954	115.035
$\alpha_{21}(C_5\text{-}N_{13}\text{-}C_{15})$	128.369	129.089	129.059	128.940	128.732
$\alpha_{22}(H_{14}\text{-}N_{13}\text{-}C_{15})$	116.825	116.061	116.046	116.106	116.233
$\alpha_{23}(N_{13}\text{-}C_{15}\text{-}O_{16})$	123.315	123.915	123.961	123.949	123.868
$\alpha_{25}(O_{16}\text{-}C_{15}\text{-}C_{17})$	121.689	121.410	121.461	121.448	121.303
$\alpha_{26}(C_{15}\text{-}C_{17}\text{-}H_{18})$	110.110	108.497	108.472	108.440	108.422
$\alpha_{27}(C_{15}\text{-}C_{17}\text{-}H_{19})$	109.816	108.496	108.472	108.440	108.422
$\alpha_{28}(C_{15}\text{-}C_{17}\text{-}H_{20})$	114.226	114.203	114.336	114.277	114.072
$\alpha_{29}(H_{18}\text{-}C_{17}\text{-}H_{19})$	105.991	107.459	107.398	107.426	107.527
$\alpha_{30}(H_{18}\text{-}C_{17}\text{-}H_{20})$	111.757	108.989	108.972	109.021	109.099
$\alpha_{31}(H_{19}\text{-}C_{17}\text{-}H_{20})$	104.466	108.989	108.973	109.021	109.100
MAE		**0.7695**	**0.7812**	**0.7736**	**0.7497**

[#]Ref.[21], crystallographic bond parameters from CIF file: CCDC No.135451.
MAE-Mean absolute error

Table 2: Structural parameters (bond lengths in Å and bond angles in degrees) of Diclofenac.

Atomic Definition	Exp. [#]	Calculated with DFT/ 6-311++G(d,p)			
		B3LYP	B3PW91	mPW1PW91	CAM-B3LYP
Bond Lengths					
$r_1(C_1\text{-}C_2)$	1.503	1.5121	1.5074	1.5047	1.5048
$r_2(C_1\text{-}O_3)$	1.216	1.2062	1.2051	1.2027	1.2015
$r_3(C_1\text{-}O_4)$	1.304	1.3545	1.3484	1.3442	1.3459
$r_4(C_2\text{-}C_5)$	1.507	1.5216	1.5152	1.5128	1.5152
$r_5(C_2\text{-}H_{20})$	1.020	1.0947	1.0952	1.0938	1.0932
$r_6(C_2\text{-}H_{21})$	0.980	1.0922	1.0934	1.0921	1.0913
$r_7(O_4\text{-}H_{22})$	0.870	0.9694	0.9678	0.9655	0.9677
$r_8(C_5\text{-}C_6)$	1.402	1.4085	1.4059	1.4033	1.4009
$r_9(C_5\text{-}C_{10})$	1.389	1.3963	1.394	1.3921	1.3899
$r_{10}(C_6\text{-}C_7)$	1.379	1.3976	1.3954	1.3933	1.3908
$r_{11}(C_6\text{-}N_{11})$	1.415	1.4241	1.4176	1.4154	1.4194
$r_{12}(C_7\text{-}C_8)$	1.376	1.3904	1.388	1.3863	1.3853
$r_{13}(C_7\text{-}H_{23})$	0.990	1.0834	1.0847	1.0835	1.0828
$r_{14}(C_8\text{-}C_9)$	1.382	1.3919	1.39	1.3881	1.386
$r_{15}(C_8\text{-}H_{24})$	0.950	1.0841	1.085	1.0836	1.0833
$r_{16}(C_9\text{-}C_{10})$	1.364	1.3925	1.3902	1.3884	1.3871
$r_{17}(C_9\text{-}H_{25})$	0.940	1.0836	1.0845	1.0831	1.0828
$r_{18}(C_{10}\text{-}H_{26})$	0.960	1.0844	1.0856	1.0844	1.0839
$r_{19}(N_{11}\text{-}C_{12})$	1.399	1.398	1.3922	1.3904	1.3956
$r_{20}(N_{11}\text{-}H_{27})$	0.750	1.0113	1.0114	1.0097	1.0101
$r_{21}(C_{12}\text{-}C_{13})$	1.390	1.4092	1.407	1.4043	1.4009
$r_{22}(C_{12}\text{-}C_{17})$	1.395	1.4099	1.4078	1.4053	1.402
$r_{23}(C_{13}\text{-}C_{14})$	1.385	1.3884	1.3866	1.385	1.3833
$r_{24}(C_{13}\text{-}Cl_{19})$	1.736	1.7629	1.7488	1.7441	1.7499
$r_{25}(C_{14}\text{-}C_{15})$	1.370	1.3907	1.3884	1.3865	1.3847
$r_{26}(C_{14}\text{-}H_{28})$	0.970	1.082	1.0831	1.0818	1.0816
$r_{27}(C_{15}\text{-}C_{16})$	1.363	1.3913	1.3889	1.3872	1.3856
$r_{28}(C_{15}\text{-}H_{29})$	0.940	1.083	1.0839	1.0826	1.0823
$r_{29}(C_{16}\text{-}C_{17})$	1.387	1.3897	1.3881	1.3863	1.3841
$r_{30}(C_{16}\text{-}H_{30})$	0.950	1.0822	1.0833	1.0819	1.0817
$r_{31}(C_{17}\text{-}Cl_{18})$	1.724	1.7518	1.738	1.7337	1.7402
MAE		**0.0107**	**0.0087**	**0.0078**	**0.0075**
Bond Angles					
$\alpha_1(C_2\text{-}C_1\text{-}O_3)$	122.40	125.679	125.592	125.542	125.640
$\alpha_2(C_2\text{-}C_1\text{-}O_4)$	114.20	111.832	111.855	111.892	112.029
$\alpha_3(O_3\text{-}C_1\text{-}O_4)$	123.30	122.488	122.553	122.564	122.329
$\alpha_4(C_1\text{-}C_2\text{-}C_5)$	110.50	113.393	113.132	112.911	113.086

$\alpha_5(C_1\text{-}C_2\text{-}H_{20})$	107.40	106.713	106.801	106.866	106.838
$\alpha_6(C_1\text{-}C_2\text{-}H_{21})$	109.20	108.662	108.734	108.792	108.755
$\alpha_7(C_5\text{-}C_2\text{-}H_{20})$	109.20	110.675	110.747	110.786	110.739
$\alpha_8(C_5\text{-}C_2\text{-}H_{21})$	111.40	108.888	108.849	108.843	108.844
$\alpha_9(H_{20}\text{-}C_2\text{-}H_{21})$	109.10	108.374	108.458	108.535	108.461
$\alpha_{10}(C_1\text{-}O_4\text{-}H_{22})$	109.00	107.231	106.895	106.990	107.410
$\alpha_{11}(C_2\text{-}C_5\text{-}C_6)$	121.20	119.568	119.565	119.507	119.308
$\alpha_{12}(C_2\text{-}C_5\text{-}C_{10})$	120.20	121.817	121.810	121.834	121.994
$\alpha_{13}(C_6\text{-}C_5\text{-}C_{10})$	118.60	118.608	118.618	118.653	118.694
$\alpha_{14}(C_5\text{-}C_6\text{-}C_7)$	119.50	119.860	119.882	119.902	119.929
$\alpha_{15}(C_5\text{-}C_6\text{-}N_{11})$	117.90	118.569	118.579	118.536	118.425
$\alpha_{16}(C_7\text{-}C_6\text{-}N_{11})$	122.60	121.559	121.526	121.552	121.639
$\alpha_{17}(C_6\text{-}C_7\text{-}C_8)$	120.60	120.568	120.542	120.511	120.481
$\alpha_{18}(C_6\text{-}C_7\text{-}H_{23})$	118.30	119.432	119.325	119.335	119.499
$\alpha_{19}(C_8\text{-}C_7\text{-}H_{23})$	120.80	119.998	120.131	120.152	120.019
$\alpha_{20}(C_7\text{-}C_8\text{-}C_9)$	120.30	120.004	120.014	120.023	120.028
$\alpha_{21}(C_7\text{-}C_8\text{-}H_{24})$	120.80	119.579	119.573	119.572	119.590
$\alpha_{22}(C_9\text{-}C_8\text{-}H_{24})$	118.90	120.409	120.405	120.397	120.376
$\alpha_{23}(C_8\text{-}C_9\text{-}C_{10})$	119.40	119.508	119.504	119.507	119.502
$\alpha_{24}(C_8\text{-}C_9\text{-}H_{25})$	116.40	120.531	120.526	120.522	120.520
$\alpha_{25}(C_{10}\text{-}C_9\text{-}H_{25})$	124.20	119.962	119.970	119.972	119.978
$\alpha_{26}(C_5\text{-}C_{10}\text{-}C_9)$	121.60	121.420	121.408	121.372	121.338
$\alpha_{27}(C_5\text{-}C_{10}\text{-}H_{26})$	118.50	119.251	119.142	119.150	119.332
$\alpha_{28}(C_9\text{-}C_{10}\text{-}H_{26})$	119.90	119.328	119.449	119.477	119.330
$\alpha_{29}(C_6\text{-}N_{11}\text{-}C_{12})$	123.10	123.682	123.464	123.127	122.909
$\alpha_{30}(C_6\text{-}N_{11}\text{-}H_{27})$	117.80	113.004	113.135	113.127	113.060
$\alpha_{31}(C_{12}\text{-}N_{11}\text{-}H_{27})$	110.60	112.180	112.173	112.230	112.460
$\alpha_{32}(N_{11}\text{-}C_{12}\text{-}C_{13})$	121.80	121.410	121.308	121.366	121.537
$\alpha_{33}(N_{11}\text{-}C_{12}\text{-}C_{17})$	121.90	122.490	122.480	122.344	122.087
$\alpha_{34}(C_{13}\text{-}C_{12}\text{-}C_{17})$	116.10	115.972	116.083	116.170	116.279
$\alpha_{35}(C_{12}\text{-}C_{13}\text{-}C_{14})$	122.50	122.758	122.684	122.632	122.553
$\alpha_{36}(C_{12}\text{-}C_{13}\text{-}Cl_{19})$	118.93	118.927	118.803	118.801	118.995
$\alpha_{37}(C_{14}\text{-}C_{13}\text{-}Cl_{19})$	118.60	118.313	118.512	118.565	118.451
$\alpha_{38}(C_{13}\text{-}C_{14}\text{-}C_{15})$	119.40	119.347	119.361	119.367	119.411
$\alpha_{39}(C_{13}\text{-}C_{14}\text{-}H_{28})$	118.10	119.535	119.460	119.435	119.436
$\alpha_{40}(C_{15}\text{-}C_{14}\text{-}H_{28})$	122.50	121.113	121.174	121.193	121.149
$\alpha_{41}(C_{14}\text{-}C_{15}\text{-}C_{16})$	120.10	119.880	119.891	119.895	119.850
$\alpha_{42}(C_{14}\text{-}C_{15}\text{-}H_{29})$	118.20	120.055	120.049	120.048	120.076
$\alpha_{43}(C_{16}\text{-}C_{15}\text{-}H_{29})$	121.60	120.061	120.055	120.052	120.070
$\alpha_{44}(C_{15}\text{-}C_{16}\text{-}C_{17})$	120.20	120.037	120.076	120.063	120.031
$\alpha_{45}(C_{15}\text{-}C_{16}\text{-}H_{30})$	125.90	120.873	120.934	120.955	120.925
$\alpha_{46}(C_{17}\text{-}C_{16}\text{-}H_{30})$	113.90	119.072	118.971	118.963	119.028
$\alpha_{47}(C_{12}\text{-}C_{17}\text{-}C_{16})$	121.60	121.953	121.847	121.817	121.832
$\alpha_{48}(C_{12}\text{-}C_{17}\text{-}Cl_{18})$	119.80	119.820	119.725	119.681	119.740
$\alpha_{49}(C_{16}\text{-}C_{17}\text{-}Cl_{18})$	118.60	118.191	118.389	118.466	118.400
MAE		**1.2980**	**1.2623**	**1.2392**	**1.2645**

Ref.[22], crystallographic bond parameters from CIF file: CCDC No.128772.

From the Table 1 and 2, it is seen that the DFT values were restrained within 0.01 Å for bond lengths and 1.3˚ for bond angles from the optimal values. The widely acknowledged standard, B3LYP showed relatively poor performance while CAM-B3LYP better performed in the prediction of structural parameters in case of both the molecules. Same inference was drawn in a similar kind of work found in the literature[24]. In the present work, we focus on the results of CAM-B3LYP level of theory for the analysis of geometrical data.

Bond lengths. From Tables1 and 2, it is found that for the N4HPA geometry, the shortest (strongest) bond is found to be Hydroxy $O_{11}\text{-}H_{12} \approx 0.961$ Å in the phenyl ring and the longest (weakest) is $C_{15}\text{-}C_{17} \approx 1.513$ Å linked with $C\text{-}CH_3$ in the acetamide moiety. In case of 2DAPA structure, the strongest bond is bridging amine $N_{11}\text{-}H_{27} \approx 0.75$ Å between two rings while, the longest (weakest) bond is found to be $C_{13}\text{-}Cl_{19} \approx 1.736$ Å, due to electronegative halogen (Cl) substituent in the dichlorophenyl ring (R_2). Further, the shortest O-H and N-H bonds confirm the stability of the titled molecules[25].

The resonating C≃C double bonds are shortened in length and also stronger than single bonds. The deviations are also correlated with the effect of electron donating substituents on the ring. For N4HPA, the computed data show that resonating C-C bond lengths fall in the range 1.389-1.396 Å (experimentally,1.395-1.402 Å). The resonating C-C bond lengths vary between 1.383-1.401Å (experimentally,1.363-1.401Å) for 2DAPA.

Bond angles and ring symmetry. Thebond anglearound N-atom,C-N-C angle for N4HPA, C_5-N_{13}-C_{15}≈128.73˚ and for 2DAPA, C_6-N_{11}-C_{12}≈122.91˚. This value is larger than the ideal tetrahedral angle (≈109.5˚) predicted for N-atom supports the possible electron delocalization in the C-N bonds of both the molecules.

The C–C–O and C-C-N bonds generally occurs around 120° gets distorted owing to resonance effect of carbon atoms as well as inter electronic interaction effect. These angles are found to be C_1-C_2-O_{11} ≈117.53˚in the hydroxy group and O_{16}-C_{15}-C_{17}≈ 121.30˚ in the acetamide fragment of N4HPA. In the carboxyl group of 2DAPA, C-C-O angles are C_2-C_1-O_4≈112.03˚ and O_3-C_1-O_4 angle is found as 122.33˚. The C-C-N bond angles in the amine fragment are computed as C_6-C_5-N_{13}≈ 117.41˚and N_{13}-C_{15}-C_{17}≈114.83˚for the N4HPA molecule. The corresponding angles are C_5-C_6-N_{11} ≈118.46˚and N_{11}-C_{12}-C_{13}≈121.54˚in 2DAPA molecule.

Owing to symmetry, the C-C-H angles in the methyl fragment must be identical[26]. However, the angles C_{15}-C_{17}-H_{20} andH_{18}-C_{17}-H_{19} are found larger than ideal value as the H_{18} and H_{19} of CH_3 lie outside the plane of symmetry of molecule.

The symmetry of the aromatic ring is distorted due to resonance effect of carbon atoms and with the inclusion of electron donating and other heavy atom fragments in the place of hydrogen atoms, yielding the internal ring angles smaller than the ideal hexagonal structure (α=120˚) and elongation of bond lengths at the point of substitution[27]. The deviation in C-C-C angles (α_i) of the ring can be analysed by estimating its root mean square value from the relation[28]:

$$RMSE_{ring} = \sqrt{\frac{\sum_i^n (\alpha_i - 120)^2}{n}} \; where, n = 6$$

The bond angles of the hexagonal rings and RMSEs are presented in Table S1(supplementary table). In case of N4HPA, the ring RMSEs for different DFT functionals vary in the range (0.868˚-0.797˚), CAM-B3LYP yields close to experimental value (~0.655˚). The asymmetry of the hexagonal ring is evidenced from the squeezing of bond angles. The observed deviation in the ring symmetry is due to inclusion of hydroxy (O_{11}-H_{12}) group at C_2 and acetamide moiety at C_5 respectively.

The 2DAPA has two phenyl rings. The Ring RMSEs fall in the range (0.87˚-0.77˚) for phenylacetic ring, R_1 and the range of RMS errors for dichlorophenyl ring, $R_2$is (2.164˚-1.941˚).The observed distortion in the ring symmetry is due to replacement of hydrogen atoms with carboxylic acid group at C_5 in ring R_1, chlorine atoms at C_{13}, C_{17} and Nitrogen at C_{12} in ring R_2. Further, it is noticed that the dichlorophenyl ring is more distorted than the phenylacetic ring. This may be reasoned as strong electron-withdrawing nature of substituents on the ring.

Dihedral angles and coplanarity. The equilibrium ground state geometry of the free molecule is planar[29]. The two parameters; C=O bond and the internal rotation angle(s) describing the intramolecular geometry of the titled molecules are closely interrelated with the characteristics of the intermolecular hydrogen bonds.

From the Table 1, it is observed that the dihedral angles δ_1-δ_{34} ≈180˚/0˚ in all DFT levels used confirming the computational coplanarity of the N4HPA molecule with its methyl fragment (δ_{35}- δ_{40}) having trigonal pyramidal molecular geometry. The experimental XRD values are slightly deviated for some fragments. These numerical deviations are discussed using CAM-B3LYP model.

The mutual orientation of the two rigid groups in N4HPA; phenyl-ring and the acetamido fragment can be characterized by the torsion (internal rotation) angle about the C_5-N_{13} axis. The significant torsion angles characterizing the coplanarity of the N4HPA are τ_1= δ_{13}(C_1-C_2-O_{11}-H_{12}), τ_2= δ_{27}(C_6-C_5-N_{13}-H_{14}), τ_3= δ_{33}(H_{14}-N_{13}-C_{15}-O_{16}), τ_4= δ_{36}(H_{19}-C_{17}-C_{15}-N_{13}).

The torsion angles τ_1,τ_2 andτ_3 are found to be nearly 180˚; an indicative of flatness of the molecule. however, these angles are deviated experimentally (≈163˚). These deviations from coplanarity are assigned as its extremely sensitiveness to hydrogen-bonding interactions, involving O-H···O and N-H···O bonds[30]. The dihedral angles in the ring are equal to 180˚ indicating that the phenyl ring is practically flat.

The methyl group orientation can be characterized by the dihedral angles δ_{35} - δ_{40}. show that the methyl H-atom (H_{20}) lies in the plane same plane (δ_{37}≈180˚),while H_{18}, H_{19} (δ_{38}≈δ_{39}≈58.2˚) are deviated from the common plane.

The spatial orientation of the diclofenac molecule is characterized by three torsion angles[31].These angles are found to be τ_1(C_5-C_6-N_{11}-C_{12}), τ_2(C_6-N_{11}-C_{12}-C_{13}) and τ_3(O_3-C_1-C_2-C_5).

The amine group (τ_1) was found to be rotated by 14.8° from the common plane of symmetry (180˚). The two aromatic rings are twisted by τ_2= -64.2° as the result repulsion interactions between the carboxylic group and the Cl atoms. This twisting enables the specific interactions of 2DAPA with the COX enzyme[32]. The carboxylic group rotated through -97.1˚ (Exp.: -68.3˚).

From the structural analysis, it is evident that most of the bond lengths and bond angles are slightlylarger than the experimental XRD values in all levels of DFT for bothN4HPA and 2DAPA. Further, these deviations are largest for bonds involving intermolecular hydrogen bonding. These discrepancies are

reasonable as the computed geometries were related to the equilibrium structures, whereas experimentally acquired geometries refer to vibrationally averaged structures[33].

Spectroscopic (FT-IR) Analysis

The harmonic wavenumbers were computed using four hybrid GGA functionals with 6-311++G(d,p) basis set have been presented in supplementary tablesS2 and S3 for the title molecules. The infrared spectra of the molecules are simulated using pure Lorentzian band shapes with FWHM of 8 cm^{-1}. The experimental (FT-IR) and B3LYP simulated spectra of the titled molecules was displayed in Fig 3a and Fig 3b.

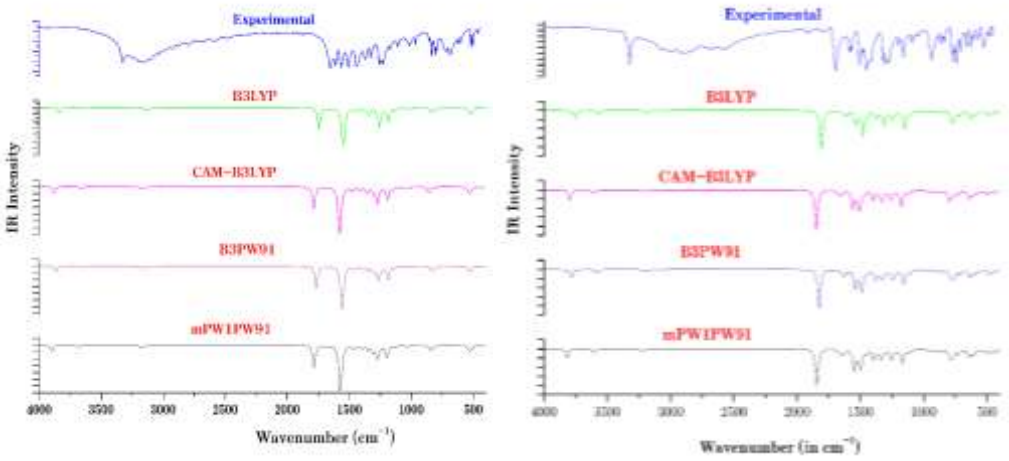

(a) Acetaminophen (b) Diclofenac

Figure 3: Experimental and simulated FT-IR spectra of (a) Acetaminophen and (b) Diclofenac.

From the Tables S2 and S3 (supplementary tables), theoretical wavenumbers are computed assuming harmonic approximation, found to be slightly overestimated. The discrepancies arise due to anharmonic effects, incomplete description of electron correlation (basis set deficiency), and probably also from the lattice effects in the samples[34]. To get a better agreement with experimental values, these wavenumbers are suitably scaled down using the specific scaling factor (SCFEM) method[34]. Further, the MAE for the computed frequencies was calculated and is found least in the case of B3LYP functional (MAE~57 and 52 cm^{-1}) and after scaling, MAE is reduced to 7 and 11 cm^{-1} for N4HPA and 2DAPA respectively showing a significant improvement. Thus, in the following discussion we present the interpretation of vibration spectra of the titled molecules through visualization of vector displacement in the Gauss view v6.1[16] and VEDA4.1e[17] program using the data acquired by B3LYP method. The experimental and scaled wavenumbers (for B3LYP) along with scaling factors and vibrational assignments with Potential Energy Distributions (PEDs) are included in Table S3a for N4HPA and in Table S3b for 2DAPA. Potential Energy Distribution (PED) analysis is a quantitative approach for the theoretical description of the contribution of vibrational motion of a given group of atoms to a particular fundamental mode[35].

According the analysis, the molecules under consideration belong to C_1 point group symmetry. Owing to this, N4HPA (20 atoms) presents 54 normal vibrational modes distributed in 36a'+18a" symmetry species. While 2DAPA (30 atoms) exhibits 84 (=56a' +28a") fundamental modes of vibrations. The characteristic descriptions of these modes based on PED matrix built on the internal coordinates were also given. The significantly high percentage of PED is attained for most of the normal modes indicating the greater stability of the molecules under C_1 symmetry. The wavenumbers predicted by the experimental FT-IR spectrum have been assigned according to the descriptions elucidated in the texts[36–39].

HydroxylGroupVibrations

The OH group gives rise to three normal vibrations stretching (ν_{OH}), in plane (β_{OH}) and out-of-plane deformations (τ_{OH}). For intermolecularly hydrogen bonded aromatics, the OH vibrations are typically observed in the region 3380±200 cm^{-1}[39] as broad and intense band depending on the extent of involvement in bonding[40]. In the present case, a weak-medium absorption band at 3326 cm^{-1} in FT-IR spectrum is assigned to OH stretching of N4HPA and the corresponding scaled (unscaled) wavenumber appeared at 3319(3837) cm^{-1} as given in Table 3. This normal mode is a pure mode with PED ~100%. The free OH in-plane (β_{OH}) bending appears in 1170±30 cm^{-1} region as a sharp peak with moderate intensity[39] which is assigned to 1172 cm^{-1} in the IR spectrum and 1168 (1186; PED~48%) in DFT calculations for N4HPA. The PED indicate that this

vibration is coupled with ring CC vibrations.The free out-of-plane (γ_{OH}) deformation labelled as torsion absorbs in the low wavenumber region 300±80 cm^{-1} [39]. The free OH torsion is observed at 273(277;95%) cm^{-1} in N4HPA. The calculated valuesare consistent with the literature[41].

C-O Vibrations. The C**–**O stretching mode coupled with C-OH in-plane deformation results in a moderate to strong band in 1245±50 cm^{-1} region and may be slightly shifted to lower side in the presence of hydrogen bonding effects[37]. The peak is computed at 1278(1284;45%) cm^{-1} at B3LYP level while its value is found at 1280 cm^{-1} in FT-IR. These values are in agreement with the results reported earlier[42].

Acetamide Group Vibrations

The 21 normal modes associated with the Acetamide (—NHC(=O)CH_3) fragment of N4HPA which are split into 13a'+8a" vibrations and described in the following paragraphs.

Acetamide NH Vibrations. It is well known that, the N–H stretching vibrations in all molecular systems occur strongly and broadly in the same absorption band ranging 3280±60 cm^{-1}[39]. In the existing effort, the strong band at 3294 cm^{-1} in the recorded FT-IR is assigned to N–H stretching. This band shows strong correlation with the predicted values 3301(3628; 100%) cm^{-1}. This peak has considerable match with the theoretical result[43]. The N-H in-plane deformation ($\beta_{C\text{-}NH}$;amide-II band), coupled with CN stretching shows a strong band in 1600-1480 cm^{-1} [39]. This band is elucidated at 1515 cm^{-1} in FT-IR and 1518(1557;48%) cm^{-1} in quantum computation. The coupled [$\omega_{(N\text{-}H)+(C=O)}$] in-phase wagging deformation leads to a broad, moderately active amide V band at 790±70 cm^{-1}[39]. This mode is implemented at 797 cm^{-1} in FT-IR and found at 790(802;12%) in B3LYP method. Analysis of the atomic displacements shows that wagging mode is strongly overlapped with other modes.

Carbonyl Vibrations. The C=O stretching, the first band in the amide group is often referred to as amide-I band in experimental spectroscopy and makes its appearance as very strong band at 1690±45 cm^{-1}[37]. This bandcomputed at 1648(1744;81%) cm^{-1} shows strong correlation with experimental value at 1655 cm^{-1} with very low intensity. The amide-IV band due to C=O in-plane, out-of-phase deformation is located at 625±70[39]. This band is computed at 627(624; 64%) cm^{-1} in B3LYP and realized at 625 cm^{-1} in experimental FT-IR. The coupled [$\gamma_{(C=O)+(N\text{-}H)}$] out-of-phase wagging deformation results in moderately intense amide-VI band at 540±80cm^{-1}[39] which is detected at 510 cm^{-1} and 514(522;67%) cm^{-1} in experimental FT-IR and theoretical DFT methods respectively.

Amide CN Vibrations. The C-N stretching (amide III band) vibration in N4HPA displays medium to strong absorption in 1160±90 cm^{-1} region[37]. The present results support the assignment of weak band at 1227 cm^{-1}in FT-IR to the C-N stretching mode. This allocationsare found to be satisfactory with literature data[44].

Methyl Vibrations. There are nine vibrational assignments associated with methyl group vibrations in the acetamide fragment of N4HPA. The CH_3stretching modes areexpected at 2990±20, 2965±35 cm^{-1} (asymmetric)and 2900±45 cm^{-1}(symmetric)[38]. The DFT values are simulated at 2944(3115), 2943(3114), and 2874(3041) for asymmetric and symmetric counterparts. The experimental IR bands are respectively assigned at 2927 cm^{-1} and 2881 cm^{-1}. The PEDs suggest thesevibrationsas pure modes and supported by the literature[45]. The methyl symmetric deformations (umbrella mode) occur as strong bands at 1365±10 cm^{-1}.In contrast, the asymmetric deformations (scissoring mode) normally exhibited at 1450±30 and 1420±20 cm^{-1} as weak to moderate bands[39]. The symmetric band appeared at 1379(1400;49%)/1371 cm^{-1} in DFT / FT-IR respectively in the present study. The asymmetric bands observed at 1468 (1490;44%), 1448(1470;77%) cm^{-1} in DFT estimations and assigned at 1442 cm^{-1} in FT-IR.The in-phase and out-of-phase rocking (ρ) modes for CH_3 vibrations overlapped with CN stretching with weak to moderate intensity displayed at 1015±95 and 1090±40 cm^{-1} respectively [39]. The IR bands identified at 1032, 979 cm^{-1} and DFT values computed at 1034(1050;22%), 998(1013;13%) cm^{-1} are assigned to CH_3 rocking modes.

Carboxylic Acid Vibrations

The 2DAPA has carboxyl (-COOH) group at ortho position of phenyl ring. There are nine normal modes associated with this group due characteristic OH, C=O and C-O vibrations which are discussed below.

OH Vibrations. The region 3150±50 cm^{-1} is the characteristic range for the quick identification of OH absorption band in carboxylic acids is observed as a very broad band in the range due to associated OH···O stretching mode. In case of 2DAPA, this band is observed at 3354 cm^{-1} in FT-IR spectrum and 3362(3756;100%) cm^{-1} in DFT calculations.The associated OH···O in-plane bending coupled with C-O stretching vibration ($\beta_{C\text{-}OH}$) is expected in the range 1395±55 cm^{-1} as moderately intense, diffused band[37,39]. This mode is observed is computed at 1366 (1373; PED~14%). The free out-of-plane (γ_{OH}) appears in the neighbourhood of 650 cm^{-1}[39]. In the IR spectrum, this peak is observed at 630 cm^{-1} for 2DAPA. The corresponding DFT computed value is 630(633;60%) cm^{-1}.

C=O Vibrations. The Carboxyl C=O stretching vibration absorbs strongly in the range 1725±65 cm^{-1}[39]. Experimentally, this mode is observed as weak peak at 1694 $cm^{-1}$is assigned to this mode and its computationally estimated value is 1694(1807;85%) cm^{-1}. This assignment is supported by the PED analysis.

C–O Vibrations. Aromatic carboxylic acids show a strong vibration in the region 1220±50 cm^{-1} as C(=O)-O stretching bandwhich is computed at 1145(1151;29) cm^{-1} using B3LYP theory. The carboxyl (C=O)-O in-plane rocking deformation appears as moderate to weak band in 395±70 cm^{-1} region[37]. The carboxyl rocking is computationally found at 410(416;71%) cm^{-1}.

Bridging Amine Vibrations

The normal vibrational modes associated with the amine NH bridge between phenylacetic and dichlorophenyl rings of 2DAPA are described as NH and CN vibrations.

NH Vibrations. The DFT calculated value of N–H stretching for bridging amine fragment of 2DAPA is found to be 3254(3568;100%) cm^{-1}. The wavenumber 3253 cm^{-1} observed in the recorded FT-IR is assigned to this mode. The N-H in-plane deformation, coupled with CH stretching shows a strong band in 1540±60 cm^{-1} and N-H out-of-plane deformation is moderately active broad band in the range 420±55 cm^{-1}[37,39]. These bands are active at 1512(1535; 23%), 460(487;42%) cm^{-1} in DFT calculations and at 1508, 461 cm^{-1} in FT-IR respectively. These bands show strong correlation with the theoretical results[6,46].

CN Vibrations. The1230±60 and 1245±55 cm^{-1} bands are linked with CN stretching vibrations the coupled with ring CH deformations for amine bridge in 2DAPA[39]. DFT values for these modes are correlated at 1222(1253;26%) and 1279(1312;51%) cm^{-1} respectively. A medium band at 1282 cm^{-1} in FT-IR is allocated to this mode.

Methylene Vibrations. The asymmetric and symmetric stretching vibrations of the methylene group are expected in the region of 2926±10 cm^{-1} and 2853±10 cm^{-1} respectively[38]. In line with this, the observed IR bands at 2925 cm^{-1} and 2890 cm^{-1}areassigned as asymmetric and symmetric counterpart of the methylene CH stretching. These values are correlated with corresponding computed values at 2922(3092;21%)and 2871(3038;79%) cm^{-1}. The scissoring mode appears as a strong peak at 1465 ± 20 cm^{-1} and that due rocking appears as very weak peat at 895±95 cm^{-1}[39]. The wagging and twisting absorptions are observed as weak bands in the region 1340±40 and 1285±45 cm^{-1} respectively[38]. In this case, the methylene deformations manifest their characteristic bands at 1454 cm^{-1} (χ), 1322 cm^{-1} (ω) and 1237 cm^{-1}(τ)in FT-IR, while rocking is absent. The DFT predictions are 1467(1482;65%), 1331(1338;19%), 1241(1247;10%)and 846(877;10%) cm^{-1} respectively.

Ring C-Cl Vibrations. In di-chlorinated aromatics, the C-Cl stretching appears as a narrow, intense bands in the range 760-395cm^{-1}[37,38] and the C-Cl in-plane and out-of-plane deformations absorb as strong-to-medium bands in the range 385–265 cm^{-1} and 390-165 cm^{-1} respectively[38]. B3LYP predicts these bands as 503(516;10%) cm^{-1} and 431(442;21%) cm^{-1} for symmetric and asymmetric C-Cl stretching respectively.

Phenyl Ring Vibrations

The normal vibrations in substituted six membered rings which are structurally very close to benzene exhibit 30 characteristic modes in 21a' and 9a'' types. The molecules under consideration; N4HPA has one 1,4-di-substituted ring while 2DAPA has two rings; phenyl-acetic (1,2 di-substituted) and dichlorophenyl (1,2,6 tri-substituted ring). Further, these modes account for 10 or 11 and 14 or 15 substituent sensitive modes in di- and tri-substituted rings[39]. The substituent sensitive (C-X) modes are also identified and assigned (TablesS3a and S3b).

Ring CH stretching. The CH stretching in the benzene ring constitutes six modes designated as 2, 20b, 20a, 13, 7b, and 7a in standard Wilson notation. In the presence of substituent; each substituent replaces one CH mode into CX mode (usually 13 or 7a in vibrational analysis).

According to the literature, ringC–H stretching vibrations are commonly appear as multiple (three or four peaks) weak bands in the region 3120–3000 cm^{-1}[38,39]. The weak FT-IR bands at 3111 cm^{-1} and 3036 cm^{-1} in N4HPA are assigned to C-H stretching modes. The scaled frequencies for these modes are computed at 3116, 3071, 3032 and 3030 cm^{-1} respectively. PEDs indicate that these modes are almost pure. In case of 2DAPA, the experimental IR bands are identified at 3071, 3029 cm^{-1} are correlated with stretching modes of CH unit in the phenylacetic ring. These stretching modes have been scaled at 3082, 3074, 3064, 3056 cm^{-1}. The corresponding modes in the dichlorophenyl ring are found at 3000, 2995, 2979 cm^{-1} in DFT and 2989 cm^{-1} in FT-IR. All CH modes are nearly pure as evidenced from PEDs shown in the Tables S3a and S3b.

Ring CH in-plane deformations. The CH in-plane deformation modes (3, 9a, 9b, 15, 18a, and 18b) in the phenyl ring are those characteristic absorptions which fall in the range 1290-990 cm^{-1} (upto six peaks) appearing as sharp but weak to medium bond, are very useful for characterisation[37]. In accord to the DFT calculations, the bands observed in the range 1320-1012 (1340-1027) cm^{-1} (Table S3a) for N4HPA are related in-plane CH bending modes. these peaks are correlated at 1303, 1179, 1108, 1015 cm^{-1} in FTIR spectrum.In the

case of 2DAPA, the in-plane CH deformation modes are estimated in the range 1278-938 (1324-972) cm^{-1} and 1184-1071 (1214-1098) cm^{-1} for phenyl acetic and dichlorophenyl rings respectively. These modes are identified at 1304, 1160, 937 cm^{-1} and 1199, 1092 cm^{-1} for the respective rings in the FT-IR spectrum. These allocations are found similar to earlier reports[1].

Ring CH out-of-plane deformations. The ring CH out-of-plane deformations (5,17a, 17b, 10a, and 11) mainly depend on the number of adjacent hydrogen atoms and not very much affected by the nature of the substituent[37].The ring CH out-of-plane bending modes are allocated in the region 880-780 cm^{-1} for disubstituted ring of N4HPA, while predicted in the range 790-720 and830-750 cm^{-1} for di- and tri-substituted rings of 2DAPA[36,37].

For N4HPA, these modes are calculated in the range 953-802(968-814) cm^{-1} computationally and in found to be active at 969, 931, 837 and 808 cm^{-1} in the experimental IR. In 2DAPA, the DFT estimated peaks in the range 956-729 (991-755) cm^{-1}, 949-756(973-775) cm^{-1} and the IR predicted peaks at 849, 741 and 766 cm^{-1} are assigned as the CH out-of-plane deformations of di- and tri-substituted rings.

Ring CC (Skeletal) Vibrations. For aromatic six membered rings, the six ring carbon atoms undergo coupled vibrations, called skeletal vibrations resulting in several split bands (upto to 6). The relevant vibrational wavenumbers are expected in region1650–1430cm^{-1}. Four of these characteristic CC stretching vibrations (νPh8a, 8b, 19a, and 19b) ideally found at 1600,1580,1490, and 1440 cm^{-1} are good group vibrations[36]. Accordingly in the present study, the CC Vibrations of N4HPA are observed as very strong the frequencies observed in the IR spectrum at 1611,1589, 1473 and 1392 cm^{-1} and theoretically predicted frequencies which are scaled at 1600, 1584, 1488, 1399 cm^{-1} are assigned to C–C stretching vibrations as shown in Table S3. In case of 2DAPA, the good group CC stretching bands are computed at 1603, 1581, 1471, 1449 cm^{-1} in ring-1 and 1599, 1584,1463,1431 cm^{-1} in ring-2. The experimental FT-IR finds these bands at 1602, 1587, 1479 cm^{-1} in ring-1 and 1577, 1568,1422,1413 cm^{-1} in ring-2. The proposed assignments arefound to be coherent with the literature[42].

The fifth mode, Kekule mode (φPh14) is active at 1315±65 cm^{-1}. The present results support these assignments related to the band observed at 1328 cm^{-1} in N4HPA and 1338, 1281 cm^{-1} for di- and tri-substituted rings of 2DAPA.The sixth mode is substituent sensitive, called the ring breathing(φPh1). In the present study, the phenyl ring of N4HPA is found to breath at dechlorinated ring is found to breath at 857 cm^{-1}, while the dechlorinated and phenyl-acetic rings of 2DAPA breath at 1045 and 1070 cm^{-1} respectively.

Skeletal deformations. The in-plane (12, 6a, 6b) and out-of-plane (4, 16a,16b) ring deformations are observed in the lower wavenumber side (<700 cm^{-1}). Three or more of them are substituent sensitive[39]. The atomic displacement vectors suggest that these modes are strongly overlapped to Ph-X stretching vibrations. PED analysis confirms this fact as most of these modes are not pure, but contain significant contributions from other modes.The proposed assignments for the skeletal deformations as shown in the Table S3a and 4 are found to be consistent with the literature[42].

Frontier Molecular Orbital (FMO) Analysis

The HOMO and LUMO together constitute the Frontier Molecular Orbitals (FMO). Fukui found a correlation with chemical activity and the electron density distribution in the frontier orbitals. He related the position of largest density of the HOMO with the site of attack of an electrophilic reagent and the distribution of the LUMO is linked with the position of nucleophilic attack[47].

The FMO Analysis of N4HPA and 2DAPA molecule was carried out with all DFT techniques described in the present work. The DFT computations of the FMO energies show significant variations in different methods. The values of all FMO energy parameters are introduced in Table 3. We focus on the B3LYP/6-311G++(d,p) level of theory for the FMO Analysis.

Table 3: FMO energies associated with Acetaminophen and Diclofenac estimated by hybrid functionals of DFT at 6-311G++(d,p) basis set.

FMO Parameters (in eV)	B3LYP	B3PW91	CAM-B3LYP	mPW1PW91
Acetaminophen				
HOMO (ψ_{40})	-5.920	-5.930	-7.284	-6.109
LUMO (ψ_{41})	-0.682	-0.651	0.118	-0.466
HOMO - LUMO Gap	5.239	5.279	7.402	5.642
Diclofenac				
HOMO (ψ_{76})	-6.132	-6.148	-7.501	-6.333
LUMO (ψ_{77})	-1.187	-1.167	0.045	-0.985
HOMO - LUMO Gap	4.945	4.981	7.546	5.348

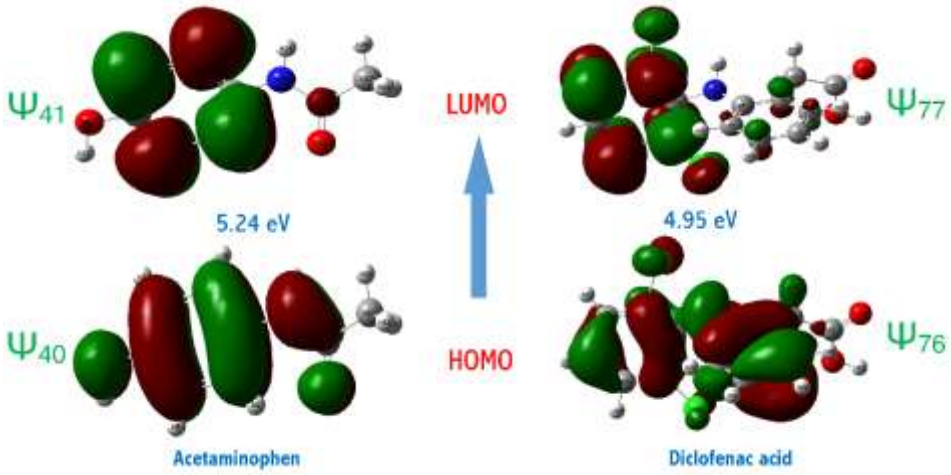

Figure 4. The orbitals contribution for the HOMO and LUMO levels simulated on the optimized structures.

The iso-density portraits for the HOMO and LUMO orbitals are plotted at an iso-surface value 0.02 au and are delineated in the Fig 4. The FMO graphic represents the atomic orbital compositions among the different fragments of the molecule where positive phase is exposed in green and negative is depicted in red which embodies the charge transfer within the molecule. The molecular orbital (MO) calculations from B3LYP theory show 40 occupied MOs for N4HPA and 76 occupied MOs in 2DAPA. From the portraits of FMOs, it is clear that the HOMO energy density of π nature in N4HPA molecule is localized over C-C bonds of Phenyl ring and C_{15}-N_{13} bond whereas the LUMO of π nature is distributed over C–C bonds in the ring and C-N bond. In case of 2DAPA, the HOMO energy density is spread across C-C bonds of both aromatic rings and amine bridge while, the LUMO surface holding π -orbital energy is localized on the dichlorophenyl ring.

From the FMO analysis, it has been observed that there is intra-molecular charge transfer from the electron donating groups (O-H, N-H and C=O group) to the benzene ring of N4PHA and intra-molecular charge transfer occurs between phenylacetic ring to dichlorophenyl ring through bridging amine fragment of 2DAPA. These π-π* interactions of FM orbitals are indicative of the molecular stability of the title molecules.

Density of States (DOS) Spectrum. The DOS plots are vital tools in understanding the electronic structure, chemical reactivity and chemical bonding.Density of states (DOS) was essentially the number of molecular orbital states at a particular energy level. The partial density of state (PDOS) describes the contribution of molecular orbital from a particular atom or fragment to the FMO of molecular system. Atom/fragment with larger percentage shares of orbitals to HOMO (LUMO) is more likely to be the preferential site of electrophilic (nucleophilic) attack[48].

In this work, the DOS spectra generated by convoluting the FMO information from the DFT output with Gaussian waveshapes of unit height and FWHM of 0.05 au using multiwfn[18] are shown in Fig5a-b and DOS plots were analyzed for the headed molecules.

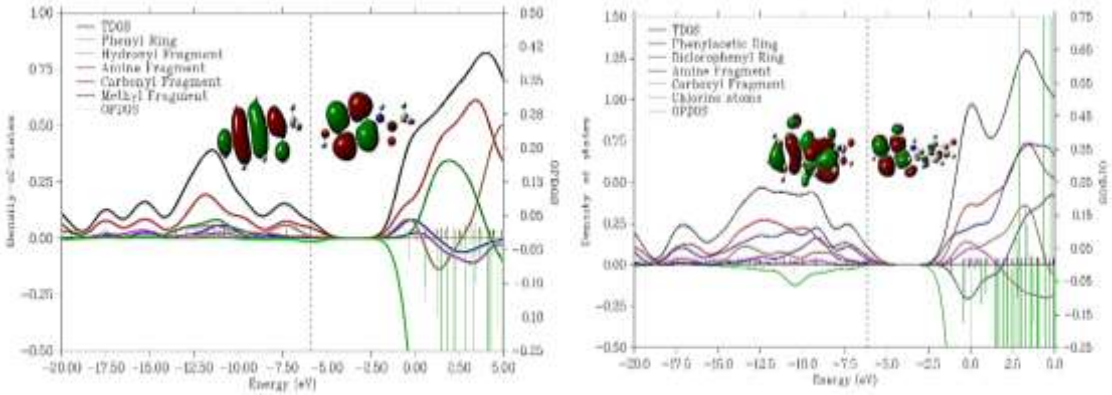

(a) (b)

Figure 5.The TDOS, OPDOS and PDOS simulated on the optimized structures in (a) Acetaminophen and (b) Diclofenac molecules.

From the DOS spectra of N4HPA, it is clear that the frontier orbitals in HOMO composed of mainly bonding interactions due to π- orbitals in ring C-C bonds (66%), along with contributions from donor fragments; hydroxy (12.3%), amine (13.5%) and acceptor fragment; carbonyl (8.1%) whereas, LUMO consists of only antibonding interactions predominated π*- orbitals in phenyl ring (98%) with insignificant contributions from other selected fragments. In case of 2DAPA, the DOS spectra predict the frontier orbitals in HOMO is formed due to bonding interactions with MO contributions from phenylacetic ring (46%), dichlorophenyl ring (26%) and donor amine (27%) fragments. The LUMO is formed due to antibonding interactions outweighed by π*- orbitals in dichlorophenyl ring (96%) while, the contributions from other fragments are negligible (Table 4).

Table 4: The individual orbital contributions (PDOS) of selected fragments on the TDOS in the frontier orbitals of acetaminophen and Diclofenac at DFT-B3LYP/6-311G++(d,p) level.

Acetaminophen			**Diclofenac**		
MO	HOMO (ψ_{40})	LUMO (ψ_{41})	MO	HOMO (ψ_{76})	LUMO (ψ_{77})
Phenyl Ring	65.7%	98.2%	Phenylacetic Ring	46.0%	2.7%
O-H	12.3%	0.2%	Dichlorophenyl Ring	25.7%	95.8%
N-H	13.5%	0.5%	N-H	26.7%	0.9%
C=O	8.1%	0.8%	COOH	0.5%	0.5%
CH_3	0.5%	0.3%	CH_2	1.1%	0.1%

The OPDOS values for occupied orbitals of N4HPA are almost zero, which predicts a weak covalent character in the molecule[49]. Further, it shows anti-bonding character in carbonyl and hydroxyl fragments in frontier HOMO of N4HPA. The OPDOS values for occupied orbitals of 2DAPA are negative in the range -12.5 to -7.5 eV which means MOs in this rangeexhibit antibonding character[50].

Global Reactivity Descriptors (GRDs). Pople and many others found that the chemical reactivity of organic molecules as a whole can be predicted by characterizing of a large number of reactivity parameters from first principles of DFT technique collectively called as global and local reactivity descriptors [51]. Within the simple molecular orbital framework, the GRDs can be expressed in more convenient way using the values of ionization potential (IP) and electron affinity (EA) which can be approximated to the frontier orbital energies by employing Koopmans' hypothesis[52] for closed-shell molecules as: $IP = -E_{HOMO}$ and $EA = -E_{LUMO}$

In the present work, DFT based global reactivity indices of the title molecules were computed using all the applied methods from the standard equations defined within the validity of the Koopman's approximation and presented in Table 5. The GRDs indicate that 2DAPA is expected to be ranked higher in terms of reaction sensitivity and softer than N4HPA molecule.When electron transfer process predominates the antioxidant activity, ionization energy can be used in qualitative comparative study of antioxidant activity [53]. As seen from Table 5, Acetaminophen may be more powerful antioxidant than Diclofenac ($I_{N4HPA} < I_{2DAPA}$).

Table 5: Global reactivity descriptors associated with acetaminophen and Diclofenac estimated using six hybrid functionals of DFT at 6-311G++(d,p) basis set.

GRD Parameter[#]	**B3LYP**	**B3PW91**	**CAM-B3LYP**	**mPW1PW91**
Acetaminophen				
Ionization Potential (IP)	5.9204	5.9302	7.2842	6.1087
Electron Affinity (EA)	0.6816	0.6512	-0.1181	0.4664
Electronegativity (χ)	3.3010	3.2907	3.5831	3.2875
Chemical Potential (μ)	-3.3010	-3.2907	-3.5831	-3.2875
Global Hardness(η)	2.6194	2.6395	3.7012	2.8211
Global Softness (σ)	0.1909	0.1894	0.1351	0.1772
Electrophilicity Index (ω)	2.0800	2.0512	1.7344	1.9155
Nucleophilic Index (ε)	-8.6466	-8.6858	-13.2618	-9.2744
Diclofenac				
Ionization Potential (IP)	6.1315	6.1479	7.5006	6.3332
Electron Affinity (EA)	1.1867	1.1666	-0.0454	0.9851
Electronegativity (χ)	3.6591	3.6572	3.7276	3.6591
Chemical Potential (μ)	-3.6591	-3.6572	-3.7276	-3.6591
Hardness(η)	2.4724	2.4907	3.7730	2.6741
Softness (σ)	0.2022	0.2008	0.1325	0.1870
Electrophilicity Index (ω)	2.7077	2.6851	1.8413	2.5035
Nucleophilic Index (ε)	-9.0468	-9.1090	-14.0642	-9.7848

[#]all values are in eV except for σ, which is in eV^{-1}.

Molecular electrostatic potential (MEP) analysis

Molecular electrostatic potential (MEP) is an effective visual method for the interpretation of the electronic structure and various aspects of chemical reactivities of the molecular systemsowing to the richness of details described by the molecular charge distributions[54].When obtained computationally, molecular electrostatic potential V(r) is typically plotted on the surface of the molecule that is defined by an outer contour of its electronic density, usually the 0.001 au (electrons/ $bohr^3$) as proposed by Bader et al.[55] which incorporate 95–98% of a molecular electronic density.

In order to visualize the overall charge distribution within the title molecules, 2-D plots of total electron density and electrostatic potential contour maps in the molecular plane (x-y plane with z=0.2 au) are generated as shown in Fig6 and Fig7 respectively. In the cross-sectional diagram for the total electron density, each contour curve around the molecule is MEP surface. The outer contour is with lower iso-surface value and inner contour is with higher iso-surface value. In case of N4HPA, contour maps indicates that O_{11}, O_{16} atoms are negatively charged because the local vdW surface bound to O_{11} and O_{16} atoms has densely populated contours and corresponds to positive MEPand the vdW contour surface around H_{12} is rarely populated. The local vdW contour surface around O_3, Cl_{18}, Cl_{19} of 2DAPA is densely populated while H_{24}, H_{25}, H_{28}, H_{29}, H_{30} are seldom populated indicating that they are protonated.

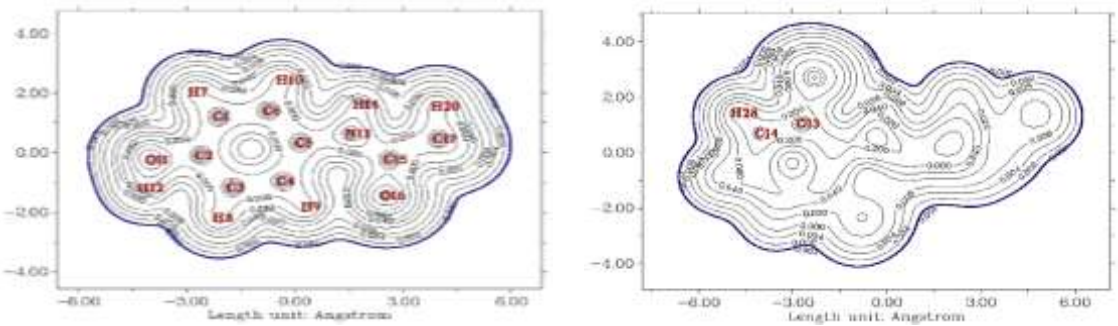

Figure 6. 2-D contour maps of total electron density in the x-y plane of (a) Acetaminophen and (b) Diclofenac.

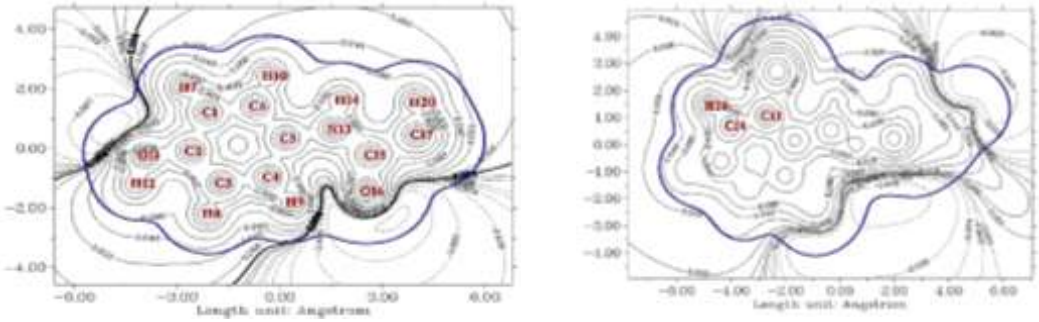

Figure 7. 2-D contour maps of electrostatic potentials in the x-y plane (with z= 0.2 au) of (a) Acetaminophen and (b) Diclofenac.

The quantitative analysisof MEP of the titled molecules have been performed using multiwfn[18] with a cubic grid spacing of 0.25 au and visual graphics displayed in Fig8 with BWR colour scheme which represents the regions of highest repulsive potential appear in red and those of highest attractive potential appear in blue.

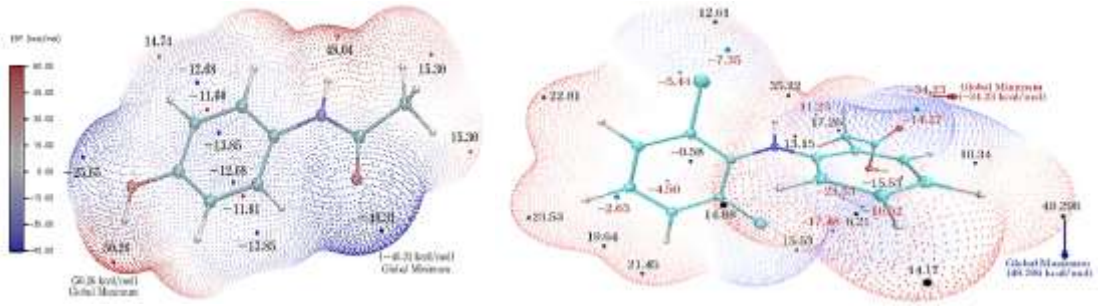

(a) (b)

Figure 8: Visual representation of MEP values at different local VdW surfaces of (a) Acetaminophen and (b) Diclofenac estimated at B3LYP level of theory.

As seen from Fig 8, it is clear that for N4HPA molecule, the global minimum i.e., The strongly negative electrostatic potential (-40.31 kcal/mol) is visible over the lone- pair regions close to O_{16} atom of the carbonyl group acts as a potential site for the electrophilic attack. The very strongly positive electrostatic potential ($V_{S,max}$ ≈+50.26 kcal/mol) is localized near the hydrogen atom (H_{12}) of the hydroxy group and $V_{S,min}$ ≈-25.65 kcal/mol of the oxygen indicate their propensities for noncovalent hydrogen bonding, as a donor and an acceptor, respectively. When focused on the 2DAPA, it was found that the strongly negative regions are associated with O_3 (-34.23 kcal/mol), O_4 (-14.27 kcal/mol) and N_{11} (11.23 kcal/mol). Thus, it is inferred that O_3, O_4 and N_{11} would be favorable sites for protonation. The positive regions of ESPs are located surrounding H-atoms which are most probable sites for nucleophilic attack.

Quantitative description of the MEP have been obtained as integral properties over this surface according to Politzer et al[56] and are presented in Table 6 and a bar graph depicting the distribution of energy densities on the molecular surface is portrayed in FigS3. The surface area corresponding to positive potential and Average ESP, averaged over positive regions ($\overline{V_S^+}$) are slightly greater than their counterparts in both the examined molecules.

Table 6: The quantitative parameters describing the molecular electrostatic surfaces of the labelled molecules.

Surface Parameters	$V_{S,max}$	$V_{S,min}$	A_S^+	A_S^-	$\overline{V_S^+}$	$\overline{V_S^-}$	σ_-^2	σ_+^2	ν	Π	MPI
N4HPA	50.26	-40.32	101.58	92.81	15.06	-13.80	121.0	101.98	0.248	14.43	14.46
2DAPA	49.30	-34.23	158.03	142.65	10.69	-9.43	71.61	64.17	0.249	10.08	10.09

From the Table 6, it is clear that, the internal charge separation (Π), $\Pi_{N4HPA}>\Pi_{2DAPA.}$which impliesN4HPA is structurally more symmetric than 2DAPA[57]. The degree of electrostatic balance (ν) for both the molecules are nearly equal to its theoretical maximum value (ν_{max}=0.250)indicating that the positive and negative surface potentials are strong and quite well balanced. The variance (σ_{tot}^2)a very useful quantity that reflects the variability of ESP. Larger the σ_-^2 andσ_+^2, the more tendency that the molecule interacts with other molecules of its own kind electrostatically. This value shows that N4HPA has relatively stronger tendency than 2DAPA. The molecular polarity index (MPI)which is closely related to the polarity index, a quite reliable index of measuring molecular polarity, the larger the index, the higher the polarity. The MPI predicts N4HPA (62.20 %) to be more polar than 2DAPA(42.51%).

Partial Charge Analysis

The partial atomic charge, is the point charge at the centre of the atom. The survey of literature reveals that it plays an important role in investigating molecular properties and predicting local (atomic sites) reactivities[58].As the charge distribution appears to be a sensitive method, in the present work, its comparison with two different approaches have been considered. the Mulliken charges are obtained by MPA with the equilibrium geometry and natural charges are obtained by NPA embedded in NBO program using the DFT/B3LYP method for the N4HPA and 2DAPA molecules as listed in Table S4. The graphical display of atomic charge distributions in the titled molecules were shown in Fig9a-b.

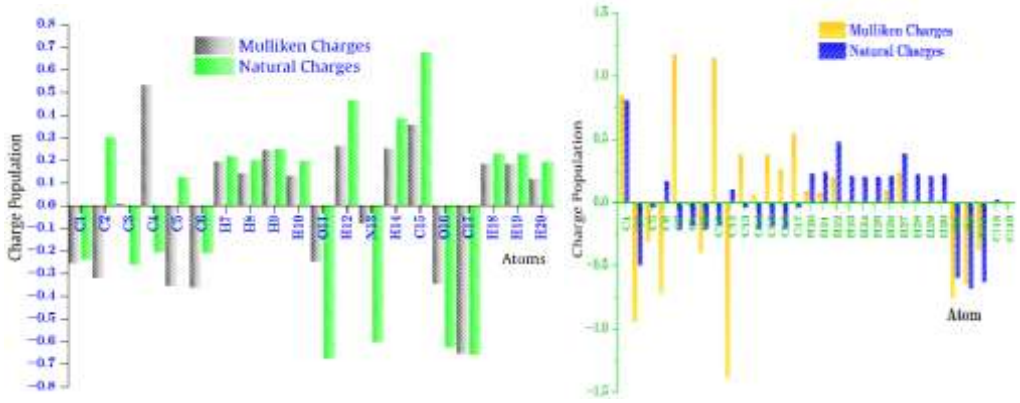

(a) (b)

Figure 9: Graphical presentation of population analysis for the outlined molecules; (a) Acetaminophen and (b) Diclofenac.

As seen from the computed values, both the analyses predict similar trends with natural charges being slightly larger than Mulliken charges for most of the atoms in both the molecules. In case of few C-atoms, contrasting values were found with MPA method. All the hydrogen atoms carry positive charge as if charge density is transferred to other atoms of the molecule and these charges lie in the range 0.1326e (H_{10}) to 0.2645 (H_{12}). The large value of positive charges on H_{12} and H_{14} may be attributed to strong intermolecular (O-H···O and N-H···O) interactions respectively. All carbon atoms carry negative charges except C_3, C_4 and C_{15} which are positiveas these atoms are bonded with heavy atoms having electronegative character. The maximum negative charge has been found on C_{17} (q=-0.6547e) in the methyl fragment which may be attributed to the hydrogens in the fragment and the maximum electron deficiency was found with C_4 atom which is a member of π-electrons in ring system. The atomic charges on heavy atoms of the functional group (-N in NH, -O in OH, C=O and -C in CH_3) are negative.

In 2DAPA molecule, all hydrogen atoms are positively charged but carbon atoms have both positive and negative charge values. The carbons bonded with electropositive hydrogens are found to be negatively charged while, those bonded with electronegative substituents are positively charged, Indicating that the delocalization of charges mainly arises through the substituent O- and N- atoms. The positive charge on hydrogen atoms is in the range: 0.0012e (H_{29}) to 0.0221e (H_{27}). This variation confirms the electron back donation from the substituent groups to phenyl rings. The obtained atomic charge shows that the carbon atom C_1 (=0.8481e) has very high positive charge than other carbons as it involved in bonding with two electronegative oxygen atoms (O_3, O_4). The oxygen (O_3=-0.7578e, O_4=-0.6521e), nitrogen(N_{11}=-0.3779e) and chlorine atoms (Cl_{18}=0.0014e, Cl_{19}=-0.0185e) are negatively charged.

Natural Bond Analysis (NBO)

In the Natural bond orbital (NBO) analysis, the second order Fock-matrix was computed which provides the insight on the donor-acceptor interactions in the NBO basis. The delocalization of electron density (ED) between the donor (i) and acceptor (j) NBO orbitals corresponds to the stabilization energy $E^{(2)}$ and is represented as:

$$E^{(2)} = \Delta E_{ij} = q_i \frac{F_{i,j}^2}{(E_i - E_j)}$$

Where i, j are the off-diagonal elements of the Fock matrix, q_i is the occupancy of the donor orbital, $F_{i,j}^2$ is the donor-acceptor interaction, and E_i, $E_j$represent the donor and the acceptor orbital energies respectively. The larger the $E^{(2)}$ value, the more intensive is the electron density transfer from the occupied lone pair electron to unoccupied acceptor electron and higher is the probability of the electron delocalization process.

The NBO calculations were performed using NBO 3.1 program[19] as implemented in the Gaussian at DFT/B3LYP level and Tables 7 and 8 show the predominanthyper-conjugative interactions and the corresponding second order perturbation energies ($E^{(2)}$) for N4HPA and 2DAPA respectively.

In case of N4HPA, strongest interaction had been observed between the orbital containing the lone electron pair; LP(N_{13}) →π* (C_{15}-O_{16}) with stabilization energies 58.73 kcal/mol. This interaction plays key role in COX- inhibition. The other important hyper-conjugative interactions include: LP(N_{13}) →π* (C_4-C_5) with $E^{(2)}$ =31.58 kcal/mol, LP(O_{11}) →π* (C_2-C_3) ; $E^{(2)}$ =26.46 kcal/mol and LP(O_{16}) →σ* (N_{13}-C_{15}) and σ*(C_{15}-C_{17}) $E^{(2)}$ =25.23, 19.01 kcal/mol respectively. Due to the different polarization coefficients, the maximum stabilization occurs with former leading to a hyper conjugative interaction[59]. Further, the electron density at the five conjugated π-bonds (~1.649–1.725e) and π*-bonds (~0.346–0.390e)of the phenyl ring distinctly exhibit strong delocalization of electron leading stabilization of the molecule ($E^{(2)}$ ~18.45–21.10 kcal/mol) and enhancement of hyperpolarizability[60].

Table 7: Predominant hyperconjugative interactions in Acetaminophen obtained from second order perturbation theory analysis of Fock matrix in NBO basis using DFT at B3LYP/6-311++G(d,p) level of theory.

Donor NBO (i)	Type	ED(i) (e)	Acceptor NBO (j)	Type	ED(j) (e)	E^a (kcal/mol)	E(j)-E(i)[b] (a.u.)	F(i,j)[c] (a.u.)
σ	C_1-C_2	1.97301	σ*	C_2-C_3	0.02700	4.02	1.27	0.064
σ	C_1-C_6	1.97417	σ*	C_2-O_{11}	0.02473	3.73	1.05	0.056
π	C_1-C_6	1.72512	π*	C_2-C_3	0.39039	19.81	0.28	0.069
σ	C_1-H_7	1.97775	σ*	C_2-C_3	0.02700	3.95	1.09	0.059
σ	C_2-C_3	1.97914	σ*	C_3-C_4	0.01409	2.87	1.30	0.054
π	C_2-C_3	1.66163	π*	C_1-C_6	0.34655	18.45	0.29	0.065

π	C_2-C_3	1.66163	π*	C_4-C_5	0.38680	21.10	0.29	0.071
σ	C_3-C_4	1.97265	σ*	C_5-N_{13}	0.03154	4.65	1.10	0.064
σ	C_3-H_8	1.97815	σ*	C_1-C_2	0.02469	3.98	1.09	0.059
σ	C_4-C_5	1.97157	σ*	C_5-C_6	0.02050	4.33	1.26	0.066
π	C_4-C_5	1.64982	π*	C_1-C_6	0.34655	21.07	0.28	0.069
π	C_4-C_5	1.64982	π*	C_2-C_3	0.39039	18.91	0.28	0.065
σ	C_4-H_9	1.97695	σ*	C_5-C_6	0.02050	4.29	1.07	0.060
σ	C_5-N_{13}	1.98728	σ*	C_{15}-C_{17}	0.05427	1.49	1.17	0.038
σ	C_6-H_{10}	1.97863	σ*	C_4-C_5	0.02270	4.18	1.10	0.061
σ	O_{11}-H_{12}	1.98745	σ*	C_1-C_2	0.02469	4.28	1.31	0.067
σ	N_{13}-H_{14}	1.98389	σ*	C_{15}-O_{16}	0.01380	4.42	1.27	0.067
σ	N_{13}-C_{15}	1.99058	σ*	C_5-N_{13}	0.03154	1.63	1.24	0.040
σ	C_{15}-O_{16}	1.99370	σ*	C_{15}-C_{17}	0.05427	1.23	1.43	0.038
π	C_{15}-O_{16}	1.99102	π*	C_{15}-O_{16}	0.28667	0.94	0.38	0.018
σ	C_{15}-C_{17}	1.98406	σ*	C_5-N_{13}	0.03154	4.47	1.05	0.061
σ	C_{17}-H_{18}	1.97672	π*	C_{15}-O_{16}	0.28667	4.24	0.53	0.045
σ	C_{17}-H_{19}	1.97673	π*	C_{15}-O_{16}	0.28667	4.24	0.53	0.045
σ	C_{17}-H_{20}	1.98925	σ*	C_{15}-O_{16}	0.01380	4.40	1.14	0.063
LP(1)	O_{11}	1.97954	σ*	C_2-C_3	0.02700	5.99	1.18	0.075
LP	O_{11}	1.88460	π*	C_2-C_3	0.39039	26.46	0.35	0.093
LP(1)	N_{13}	1.67162	π*	C_4-C_5	0.38680	31.58	0.30	0.088
LP(1)	N_{13}	1.67162	π*	C_{15}-O_{16}	0.28667	58.73	0.28	0.117
LP(1)	O_{16}	1.97750	σ*	C_{15}-C_{17}	0.05427	2.01	1.05	0.041
LP	O_{16}	1.86492	σ*	N_{13}-C_{15}	0.07731	25.23	0.70	0.120
LP	O_{16}	1.86492	σ*	C_{15}-C_{17}	0.05427	19.01	0.62	0.099
LP(1)	O_{16}	1.97750	σ*	C_4-H_9	0.01423	0.60	1.16	0.02
LP	O_{16}	1.86492	σ*	C_4-H_9	0.01423	1.14	0.73	0.03
LP	O_{16}	1.86492	σ*	C_{17}-H_{20}	0.00594	0.62	0.64	0.02
π*	C_{15}-O_{16}	0.28667	π*	C_4-C_5	0.38680	1.31	0.02	0.007
π*	C_{15}-O_{16}	0.28667	σ*	C_{17}-H_{18}	0.00585	1.24	0.38	0.051

ED – Electron Density; LP – Lone Pair.

[a] E means energy for hyperconjugative interactions (stabilization energy).

[b] Energy difference between donor (i) and acceptor (j) NBO orbitals.

[c] F(i,j) is the Fock matrix element between i & j NBO orbitals.

Table 8: Predominant hyperconjugative interactions in Diclofenac obtained from second order perturbation theory analysis of Fock matrix in NBO basis using DFT at B3LYP/6-311++G(d,p) level of theory.

Donor NBO (i)	Type	ED(i) (e)	Acceptor NBO (j)	Type	ED(j) (e)	E[a] (kcal/mol)	E(j)-E(i)[b] (a.u.)	F(i,j)[c] (a.u.)
σ	C_1-C_2	1.97799	σ*	C_5-C_6	0.02981	2.34	1.22	0.048
σ	C_1-O_3	1.99679	σ*	C_1-C_2	0.05865	1.36	1.47	0.041
π	C_1-O_3	1.99179	σ*	C_2-C_5	0.02187	1.44	0.80	0.03
σ	C_1-O_4	1.99575	σ*	C_2-H_{20}	0.01502	0.62	1.33	0.026
σ	C_2-C_5	1.96453	σ*	C_6-C_7	0.02506	3.04	1.20	0.054
σ	C_2-H_{20}	1.96511	π*	C_5-C_{10}	0.35384	4.01	0.55	0.046
σ	C_2-H_{21}	1.96798	σ*	C_1-O_3	0.02299	3.84	1.12	0.059
σ	O_4-H_{22}	1.98630	σ*	C_1-C_2	0.05865	3.80	1.13	0.059
σ	C_5-C_6	1.96724	σ*	C_6-C_7	0.02506	4.12	1.27	0.065
σ	C_5-C_{10}	1.97191	σ*	C_6-N_{11}	0.03070	4.14	1.10	0.06
π	C_5-C_{10}	1.67435	σ*	C_2-H_{20}	0.01502	3.32	0.64	0.045
π	C_6-C_7	1.65459	π*	C_8-C_9	0.34382	21.04	0.29	0.07
σ	C_7-C_8	1.97583	σ*	C_6-N_{11}	0.03070	4.49	1.10	0.063
σ	C_7-H_{23}	1.97716	σ*	C_5-C_6	0.02981	4.44	1.08	0.062
σ	C_8-C_9	1.97898	σ*	C_7-C_8	0.01458	2.79	1.28	0.053
π	C_8-C_9	1.66377	π*	C_5-C_{10}	0.35384	21.63	0.28	0.07
σ	C_8-H_{24}	1.98027	σ*	C_6-C_7	0.02506	3.85	1.08	0.058
σ	C_9-C_{10}	1.97705	σ*	C_2-C_5	0.02187	3.78	1.10	0.057
σ	C_{10}-H_{26}	1.97875	σ*	C_5-C_6	0.02981	4.49	1.08	0.062
σ	N_{11}-C_{12}	1.98492	σ*	C_{12}-C_{17}	0.04084	2.08	1.33	0.047
σ	N_{11}-H_{27}	1.97493	π*	C_6-C_7	0.38274	2.46	0.67	0.04
σ	C_{12}-C_{13}	1.96859	σ*	C_{12}-C_{17}	0.04084	4.50	1.26	0.067
π	C_{12}-C_{13}	1.67030	π*	C_{14}-C_{15}	0.34478	20.06	0.30	0.07
σ	C_{12}-C_{17}	1.96669	σ*	C_{12}-C_{13}	0.04033	4.54	1.26	0.068
σ	C_{13}-C_{14}	1.97878	σ*	C_{12}-C_{13}	0.04033	3.81	1.26	0.062

σ	C_{13}-Cl_{19}	1.98615	σ*	C_{12}-C_{17}	0.04084	2.57	1.24	0.051
σ	C_{14}-C_{15}	1.97036	σ*	C_{13}-Cl_{19}	0.03058	5.08	0.84	0.058
π	C_{14}-C_{15}	1.66846	π*	C_{16}-C_{17}	0.38959	22.69	0.27	0.071
σ	C_{14}-H_{28}	1.97759	σ*	C_{12}-C_{13}	0.04033	4.71	1.06	0.063
σ	C_{15}-C_{16}	1.97154	σ*	C_{16}-C_{17}	0.02397	3.75	1.27	0.062
σ	C_{15}-H_{29}	1.97888	σ*	C_{16}-C_{17}	0.02397	3.47	1.09	0.055
σ	C_{16}-C_{17}	1.97899	σ*	C_{12}-C_{17}	0.04084	3.77	1.26	0.062
π	C_{16}-C_{17}	1.69661	π*	C_{12}-C_{13}	0.45289	21.13	0.28	0.071
σ	C_{16}-H_{30}	1.97760	σ*	C_{17}-Cl_{18}	0.02803	5.29	2.51	0.103
σ	C_{17}-Cl_{18}	1.98593	σ*	C_{12}-C_{13}	0.04033	2.49	1.24	0.05
LP(1)	O_3	1.97718	σ*	C_1-C_2	0.05865	2.57	1.08	0.047
LP	O_3	1.85185	σ*	C_1-O_4	0.10124	33.51	0.61	0.129
LP(1)	O_4	1.97746	σ*	C_1-O_3	0.02299	6.81	1.24	0.082
LP	O_4	1.82031	π*	C_1-O_3	0.20260	44.61	0.35	0.112
LP(1)	N_{11}	1.78857	π*	C_{12}-C_{13}	0.45289	21.53	0.28	0.074
LP(1)	Cl_{18}	1.99227	σ*	C_{16}-C_{17}	0.02397	1.73	1.49	0.046
LP	Cl_{18}	1.96633	σ*	C_{12}-C_{17}	0.04084	5.07	0.84	0.058
LP	Cl_{18}	1.92227	π*	C_{16}-C_{17}	0.38959	12.46	0.32	0.061
LP(1)	Cl_{19}	1.99263	σ*	C_{13}-C_{14}	0.02391	1.49	1.50	0.042
LP	Cl_{19}	1.96541	σ*	C_{12}-C_{13}	0.04033	4.39	0.86	0.055
LP	Cl_{19}	1.96541	σ*	N_{11}-H_{27}	0.02277	1.11	0.73	0.025
LP	Cl_{19}	1.93261	π*	C_{12}-C_{13}	0.45289	11.48	0.33	0.061
π*	C_6-C_7	0.38274	σ*	N_{11}-H_{27}	0.02277	1.15	0.36	0.040
π*	C_{12}-C_{13}	0.45289	π*	C_{14}-C_{15}	0.34478	144.21	0.02	0.081
π*	C_{16}-C_{17}	0.38959	π*	C_{14}-C_{15}	0.34478	225.41	0.01	0.085

In case of 2DAPA, strongest interaction occurred between the orbital containing the lone electron pair; LP(O_4) →π* (C_1-O_3); $E^{(2)}$ =44.61 kcal/mol. This hyper-conjugative interaction is responsible for its bio and pharmaceutical activity. The other significant lone pair interactions include: LP(O_3) →π* (C_1-O_4); $E^{(2)}$ =33.51 kcal/mol, LP(N_{11}) →π* (C_{12}-C_{13}); $E^{(2)}$ =21.53 kcal/mol, LP(Cl_{18}) →π* (C_{16}-C_{17}); $E^{(2)}$ =12.46 kcal/mol, LP(Cl_{19}) →π* (C_{12}-C_{13}); $E^{(2)}$ =11.48 kcal/mol. Also, two strong π→π* interactions (C_6-C_7)→ (C_8-C_9); $E^{(2)}$ =21.04 kcal/mol, (C_8-C_9) → (C_5-C_{10}) ; $E^{(2)}$ =21.63 kcal/mol in the phenylacetic ring and three prominent π→π* interactions (C_{14}-C_{15})→ (C_{16}-C_{17}), (C_{16}-C_{17})→ (C_{12}-C_{13}), (C_{12}-C_{13}) →(C_{14}-C_{15}) with energies 22.69, 21.13, 20.06 kcal/mol respectively in the dichlorophenyl ring have been observed. In addition, the π*→π* interactions (C_{16}-C_{17})→ (C_{14}-C_{15}) and (C_{12}-C_{13}) →(C_{14}-C_{15}) with $E^{(2)}$ =225.41 and 144.21kcal/mol respectively exhibit strong delocalization of electron in the dichlorophenyl ring. These conjugative interactions result in intra-molecular charge transfer (ICT) leading to stabilization of the molecule and responsible for bioactivity[61].

NBO analysis also revealed that the oxygen lone pair (O_{16}) in N4HPA donate its electrons to σ-type anti-bonding orbitals (C_4-H_9) and (C_{17}-H_{20}) with stabilization energies 1.14 and 0.62 kcal/mol respectively. These weak NBO interactions suggest the probable C–H···O intermolecular hydrogen bonding. In 2DAPA, significant weak lone pair interaction corresponds to LP(Cl_{19}) →σ* (N_{11}-H_{27}); $E^{(2)}$ =1.11kcal/mol in its secondary amino group. This weak hyper-conjugative interaction results in N-H···Cl hydrogen bond[22].

Non-Linear Optical (NLO) Properties

The polarizability (α) and hyperpolarizability (β, γ) characterize the response of a system in an applied electric field.According to Buckingham's definitions, DFT has been used as an effective tool to comprehendthe NLObehaviour. The NLO Parametersof the chosen molecules were calculated by finite field approach using the relations explained previously[62]from Gaussian output using B3LYP and CAM-B3LYP functionals. These NLO parameters were reported in Table 9 and theirtensor components are listed in Table S5 (supplementary material).

Table 9: Static NLO Parameters of acetaminophen and Diclofenac molecules computed using hybrid functionals of DFT at 6-311++G(d,p) basis set. (All values of μ, α, β and γ are in $\times10^{-18}$ esu, $\times10^{-25}$ esu, $\times10^{-33}$ esu and $\times10^{-37}$ esu respectively).

NLO Parameter	Acetaminophen		Diclofenac	
	B3LYP	CAM-B3LYP	B3LYP	CAM-B3LYP
Total dipole moment(μ_{total})	2.2738	2.3352	2.8029	2.9194
Average isotropic polarizability⟨$\boldsymbol{\alpha}$⟩	167.5622	161.1591	306.8195	295.6717
Anisotropy of polarizability (Δα)	129.0893	117.8329	141.9991	130.9664
Total first hyperpolarizability (β_{total})	7313.913	4963.297	4457.383	3495.169
Average first hyperpolarizability⟨$\boldsymbol{\beta}$⟩	-1128.562	-949.782	-2616.745	-1952.956

Projection of βon dipole moment($\boldsymbol{\beta_V}$)	-677.137	-569.869	-4361.242	-3254.926
Parallel component of β: $\boldsymbol{\beta_{\parallel}}(\boldsymbol{z})$	-0.144	-0.117	-383.546	-644.668
perpendicular component of β: $\boldsymbol{\beta_{\perp}}(\boldsymbol{z})$	-0.048	-0.039	-127.849	-214.889
Total second hyperpolarizability(γ_{total})	148.335	102.363	222.428	156.782
Average second hyperpolarizability$\langle\boldsymbol{\gamma}\rangle$	202.720	146.000	349.973	253.207
Normal component of γ : $\boldsymbol{\gamma_{\perp}}$	67.573	48.667	116.658	84.402

$\beta_{\parallel}(z)$ - Parallel component of βabout z-axis; $\beta_{\perp}(z)$ - perpendicular component of βabout z-axis.
$\gamma_{\perp}$-Normal component about the standard orientation of second hyperpolarizability (γ).

From the tables, it is found that the highest value of μ is observed for the component μ_y in case of N4HPA and μ_x in case of 2DAPA.On comparison of dipole moments, it is observed that $\mu_{N4HPA}<\mu_{2DAPA}$. This result shows that 2DAPA is more asymmetric than N4HPA[17]. The calculated α_{ij} has nonzero values and is dominated by the diagonal components for both the molecules.

The computed hyperpolarizability values (β, γ) for CAM-B3LYP are 68%, 69% and 78%, 70% of those obtained from B3LYP for N4HPA and 2DAPA respectively.For both the headed molecules, the value of β_{xxx} component is found to be largest which indicates that the molecules have major component of polarizability along axial direction. This large hyperpolarizability value is directly correlated charge delocalization from donor to acceptor through π conjugated framework[63].

The value of γ mainly depends on the factors such as the extent of π-electron conjugation, substituted functional groups and dimensionality of the molecules[1]. The dominant component for the magnitude of γ is γ_{xxxx} (= 631.164 $\times10^{-37}$ esu for N4HPA and 706.422$\times10^{-37}$ esu for 2DAPA; Table S8) for both the molecules. The magnitude of γ for 2DAPA is larger than that of N4HPA and hence possess better third-order optical nonlinearity.

Urea is the perfect NLO moleculeand is one of the exemplary molecules frequently considered as a threshold for comparison of the NLO properties of the molecular systems[64]. On comparing with the standard values of Urea, the dipole moments are greater by 1.7 times for N4HPA and 2 times in case of 2DAPA (μ_{urea}=1.3732 D). The average linear polarizability (α_{total}) of N4HPA and 2DAPA are respectively larger by 4.4 times and 8 times than that of Urea (α_{urea}=38.312$\times10^{-25}$esu). Also, the average first hyperpolarizability, β_{total} showedsignificant increase. The value is20 times and 12 times larger than that of Urea (β_{urea}=372.89$\times10^{-33}$esu) for N4HPA and 2DAPA are respectively. These results suggest that the title compounds be attractive materials for future studies of non-linear properties.

AIM-Topology Analysis

In the framework of Bader's Quantum Theory of Atoms in Molecules (QTAIM), various inter- and intra-molecular interactions between donor and acceptor atoms were explored, owing to their significant influence on the reactivity of the biological systems[65]. The approach is to link the maximum gradient path (Bond Path) through bond critical point (BCP), a representative point with appropriate local density maxima and describe a number of topological parameters at BCP; charge density (ρ_{BCP}) and its Laplacian ($\nabla^2\rho_{BCP}$), local Lagrangian kinetic energy density (G_{BCP}), local potential energy density (V_{BCP}), total electron energy density (H_{BCP}), interaction energy (ΔE_{int}) of atomic bonds for efficient detection and quantification of the interactions[66].

Table 10: AIM-Topology parameters about the Bond Critical Point (BCP); electron density (ρ_{BCP}), Laplacian of electron density ($\nabla^2\rho_{BCP}$), Lagrangian kinetic energy (G_{BCP}), local potential electron energy density (V_{BCP}), total electron energy density (H_{BCP}) and estimated interaction energy (E_{int}) of atomic bonds of N4HPA and 2DAPA.

Bonding Atoms	ρ_{BCP} (au)	$\nabla^2\rho_{BCP}$ (au)	G_{BCP} (au)	V_{BCP} (au)	H_{BCP} (au)	$\frac{H_{BCP}}{\rho_{BCP}}$	$\frac{\lvert V_{BCP}\rvert}{G_{BCP}}$	ΔE_{int} (kcal/mol)
N4HPA								
C_4-H_9···O_{16}	0.0177	0.0646	0.0140	-0.0118	0.0022	0.1243	0.8429	-3.7032
2DAPA								
N_{11}-H_{27}···Cl_{19}	0.0158	0.0650	0.0136	-0.0109	0.0027	0.1709	0.8015	-3.4207

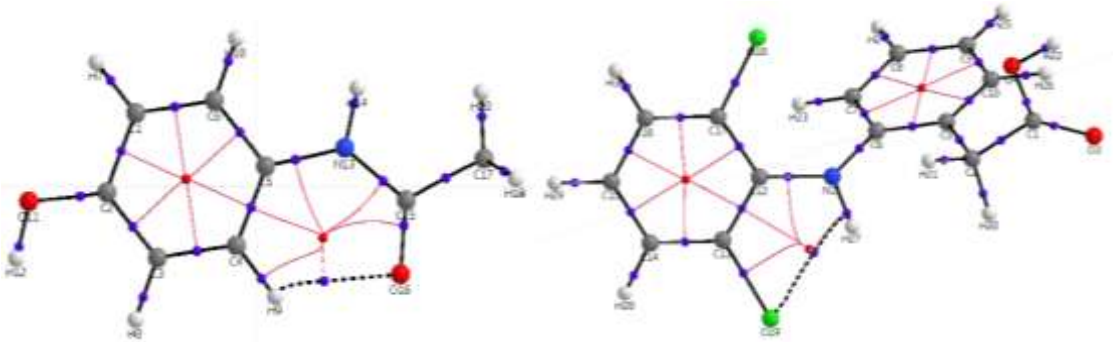

Fig. 10:Molecular graph of critical points and bond paths in (a) acetaminophen and (b) diclofenac; red spots correspond to ring critical points (RCP) and blue ones denote bond critical points (BCP).

As expected, 21 BCPs /32 BCPs associated with the standard covalent bonds in N4HPA/ 2DAPA respectively were found, including RCPs at the centroid of benzene ring. In addition, one extra BCP was predicted, owing to weak intramolecular interactions, which in turn generate one more RCP.Table 10 have been reported for the topological descriptors the selected BCPs associated with the studied molecules. Fig. 10(a) and 10(b) display the molecular graphs showing non-bonded interactions represented by BCPs in case of N4HPA and 2DAPA respectively. The aromatic C—C and C—H bonds and some polar bonds have the expected topological properties and merit no further comment. It revealed one BCP between non bonded atoms between the atomic centres$H_9\cdots O_{16}$in N4HPA and one BCP between $H_{27}\cdots Cl_{19}$ in 2DAPA. These weak interactions are characterized by very small values of $\rho(r)$, small positive values of $\nabla^2\rho_{BCP}$, high values of ε and λ_3 (relative to λ_1, λ_2), nearly zero values of H_{BCP} and values of $|V_{BCP}|/G_{BCP}$ generally ≤ 1. These values are consequence of the high sensitivity of the local energetic properties at interaction geometries which are associated with the atoms. The C-H…O intramolecular bonds have values of $\rho(r)$ and $\nabla^2\rho_{BCP}$ are well within the recommended range by Koch and Popelier[67]. Also, the positive values of $\nabla^2\rho$ imply that both of the bonds are closed-shell in nature.In terms of the Espinosa classification[68], these weak intramolecular interactions overlap between the type III pure closed-shell zone and the type V transit zone. The estimated interaction energy for H-bond was found to be 3.70 and 3.42 kcal/mole for N4HPA and 2DAPA respectively indicating that former chemically more reactive.

Non-Covalent Interaction (RDG-NCI) Analysis

For further insights into the nature of the possible intramolecular interactions in the titled molecules, non-covalent interaction (NCI) analysis, proposed by Johnson et al[69] was performed utilizing Multiwfn code developed by Lu and Chen [18]. The NCI Analysis is a modification of RDG approach for examining noncovalent interactions has been to assign van der Waals interactions (vdW), steric clashes (SC), and hydrogen bonds (HBs) in terms of the values of sign $(\lambda_2)\rho$, the electron density multiplied by the sign of the second Hessian eigenvalue.

The nature and strength of molecular interactions can be visually revealed by the NCI-Plot, a scattered graph (Fig 11) obtained by representing values of sign $(\lambda_2)\rho$ on BGR colour scale, ranging from -0.035 to 0.02 au and mapping onto RDG iso-surface. each point in the graph corresponds to a grid point in 3D space. There are several spikes, the points at their peaks are just the approximate CP positions in AIM theory.

From the colour-filled NCI-Plot (for RDG isosurface=0.5 au), the domains of the low density, low-gradient lying at negative values (blue spikes) are indicative of strong attractive (stabilizing) interactions. Conversely, the domains of the low density, low-gradient that remains at positive values (red spikes) indicate strong repulsive interactions (nonbonded overlap) in the central area of the sterically crowded molecule. Finally, the domains of the low-density, low-gradient (green or light brown spikes) very near zero, with slightly negative values, indicative of weak vdW (attractive) interactions[70].

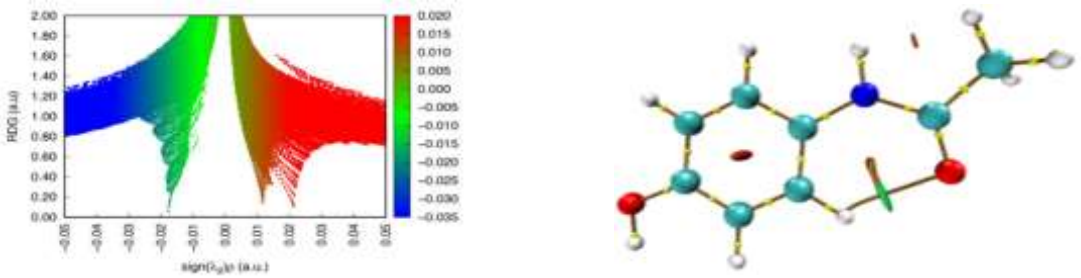

(a) Acetaminophen

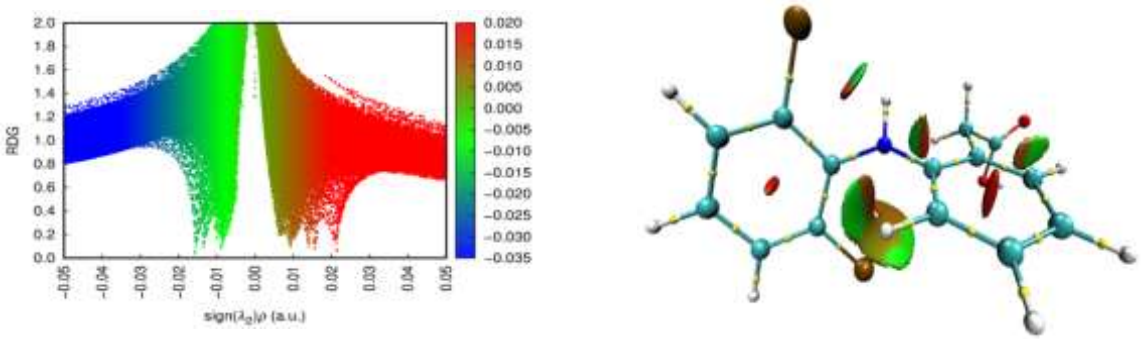

(b) Diclofenac

Figure 11: 2D scatter graph (left) and the 3D color-filled RDG isosurfaces (right) representing non-covalent interactions in the optimized structures of (a) N4HPA and (b) 2DAPA molecules.

According to our calculations, there are no strong hydrogen bonding interactions. However, a number of stabilizing intramolecular nonbonding interactions such as VdW interactions and the steric effects in the compound. In case of N4HPA, there exist one intra-molecular VdW type of attraction (C-H…O) between H_9 and O_{16}. For 2DAPA molecule, weak stabilizing VdW interaction between H_{27} and Cl_{19} bonding was predicted. From RDG isosurface plot red colour flaky patches inside the rings of both the molecules indicate the strong steric clashes which is also evident from the scatter plots between the region 0.01–0.02 a.u.Apparently, all bonding interactions in both the molecules are found to be weak, indicating that they might be biologically active.NCI analysis shows that the regions of steric clashes are more pronounced in 2DAPA than in case of N4HPA which accounts for the low stability of former molecule. The AIM and NCI analysis give more insights into the nature of different types of interactions, both attractive and repulsive in nature leading to the stabilization of the structure.

IV. Conclusions

Here we presented a systematic DFT analysis on Acetaminophen and Diclofenac molecules. Within the computational limits, the optimized geometric parameters are found consistent with multiple published XRD data for identical geometries.The slight variations in these parameters wereattributed to probable intermolecular interactions. Further, molecular asymmetry has been invoked from the structural analysis. DFT calculations expediently enabled us to interpret the experimental FT-IR data by assigning the computed frequencies within the framework of the group frequencies. The comprehensive vibrational analysis was performed on the basis of PEDmatrix. The chemical reactivity of the molecules was discoursed using FMO and DOS analysis and various GRDs were estimated and it was found that Acetaminophen may be more powerful antioxidant than Diclofenac. The large difference in HOMO and LUMO energy supports the charge – transfer model of interaction within the molecule. MEP reveals that the C=O bond is the most probable site for electrophilic attackin both the molecules. Further, quantitative description of the MEP shows thatN4HPA is structurally more symmetric than 2DAPA.The results of NBO analysis illustrate that lone pair interactions are relatively strong hyper-conjugative interactions and responsible for pharmaceutical activity and structural stability.NBO scheme also suggests that the intramolecular charge transfer along conjugated ring path enhances NLO activity. The hyperpolarizability values show that the titled compoundspossess considerable NLO responses, larger than that of Urea andare suitable materials for further NLO studies.According to AIM and NCI calculations, all H-bonds are found to be weak and there exist one weak stabilizing intra-molecular H-bond in N4HPA and 2DAPA. Further, the estimated interaction energy for H-bond is 3.70 and 3.42 kcal/mole for N4HPA and 2DAPA respectively. Thus, the enhanced H-bonding in N4HPA may suggest that it is chemically more reactive as compared to 2DAPA.

References

[1] E.B. Burgina, V.P. Baltakhinov, E. V. Boldyreva, T.P. Shakhtschneider, Ir Spectra Of Paracetamol And Phenacetin. 1. Theoretical And Experimental Studies, J. Struct. Chem. 2004 451. 45 (2004) 64–73. https://doi.org/10.1023/B:Jory.0000041502.85584.D5.

[2] N. Okulik, A.H. Jubert, Theoretical Study On The Structure And Reactive Sites Of Non-Steroidal Anti-Inflammatory Drugs, J. Mol. Struct. Theochem. 682 (2004) 55–62. https://doi.org/10.1016/J.Theochem.2004.04.069.

[3] K.Y. Ho, K.A. Gwee, Y.K. Cheng, K.H. Yoon, H.T. Hee, A.R. Omar, Nonsteroidal Anti-Inflammatory Drugs In Chronic Pain: Implications Of New Data For Clinical Practice, J. Pain Res. 11 (2018) 1937–1948. Https://doi.org/10.2147/Jpr.S168188.

[4] J.A. Cordero, M. Camacho, R. Obach, J. Domenech, L. Vila, In Vitro Based Index Of Topical Anti-Inflammatory Activity To Compare A Series Of Nsaids, Eur. J. Pharm. Biopharm. 51 (2001) 135–142. Https://doi.org/10.1016/S0939-6411(00)00149-1.

[5] J.R. Vane, R.M. Botting, Mechanism Of Action Of Aspirin-Like Drugs, Semin. Arthritis Rheum. 26 (1997) 2–10. https://doi.org/10.1016/S0049-0172(97)80046-7.

[6] A. Jubert, N.E. Massa, L.L. Tévez, N.B. Okulik, Vibrational And Theoretical Studies Of The Non-Steroidal Anti-Inflamatory

Drugs Niflumic [2-3((3-Trifluoromethyl)Phenyl Amino)-3-Pyridinecarboxylic Acid]; Diclofenac [[2-(2,6-Dichlorophenyl)Amino]-Benzene Acetic Acid] And Indometacin Acids [1-(4-Chloroben, Vib. Spectrosc. 37 (2005) 161–178. https://doi.org/10.1016/J.Vibspec.2004.08.005.

[7] W.M. Lee, Acetaminophen (Apap) Hepatotoxicity—Isn't It Time For Apap To Go Away?, J. Hepatol. 67 (2017) 1324–1331. https://doi.org/10.1016/J.Jhep.2017.07.005.

[8] J.J. Lee, D.L. Simmons, Antipyretic Therapy: Clinical Pharmacology, Handb. Clin. Neurol. 157 (2018) 869–881. https://doi.org/10.1016/B978-0-444-64074-1.00054-9.

[9] N. V. Chandrasekharan, H. Dai, K.L.T. Roos, N.K. Evanson, J. Tomsik, T.S. Elton, D.L. Simmons, Cox-3, A Cyclooxygenase-1 Variant Inhibited By Acetaminophen And Other Analgesic/Antipyretic Drugs: Cloning, Structure, And Expression, Proc. Natl. Acad. Sci. U. S. A. 99 (2002) 13926–13931. https://doi.org/10.1073/Pnas.162468699.

[10] B. Cryer, M. Feldman, Cyclooxygenase-1 And Cyclooxygenase-2 Selectivity Of Widely Used Nonsteroidal Anti-Inflammatory Drugs, Am. J. Med. 104 (1998) 413–421. https://doi.org/10.1016/S0002-9343(98)00091-6.

[11] P. Pantziarka, V. Sukhatme, G. Bouche, L. Meheus, V.P. Sukhatme, Repurposing Drugs In Oncology (Redo)—Diclofenac As An Anti-Cancer Agent, Ecancermedicalscience. 10 (2016).

[12] S.D. Malhotra, D.A. Rana, V.J. Patel, Comparison Of Analgesic, Anti-Inflammatory And Anti-Pyretic Efficacy Of Diclofenac, Paracetamol And Their Combination In Experimental Animals, Int. J. Basic Clin. Pharmacol. 2 (2013) 458. https://doi.org/10.5455/2319-2003.Ijbcp20130821.

[13] G. Akhavanakbari, M. Entezariasl, K. Isazadehfar, F. Kahnamoyiagdam, The Effects Of Indomethacin, Diclofenac, And Acetaminophen Suppository On Pain And Opioids Consumption After Cesarean Section, Perspect. Clin. Res. 4 (2013) 136. https://doi.org/10.4103/2229-3485.111798.

[14] G. Rauhut, Recent Advances In Computing Heteroatom-Rich Five- And Six-Membered Ring Systems, Adv. Heterocycl. Chem. 81 (2001) 1–105. https://doi.org/10.1016/S0065-2725(01)81010-2.

[15] M.J. Frisch, G.W. Trucks, H.B. Schlegel, G.E. Scuseria, M.A. Robb, J.R. Cheeseman, G. Scalmani, V. Barone, B. Mennucci, G.A. Petersson, H. Nakatsuji, M. Caricato, X. Li, H.P. Hratchian, A.F. Izmaylov, J. Bloino, G. Zheng, J.L. Sonnenberg, M. Had, D.J. Fox, Gaussian 09 C.01, Gaussian 09, Rev.C.01; Gaussian, Inc. Wallingford Ct, 2010. (2010).

[16] R.D. Dennington Ii, A. Keith,Todd, M.M. John, Gaussview, Version 6.0.16, (2016) Semichem Inc., Shawnee Mission Ks.

[17] M.H. Jamróz, Vibrational Energy Distribution Analysis Veda 4, Spectrochim. Acta Part A Mol. Biomol. Spectrosc. 114 (2013).

[18] T. Lu, F. Chen, Multiwfn: A Multifunctional Wavefunction Analyzer, J. Comput. Chem. 33 (2012) 580–592. https://doi.org/10.1002/Jcc.22885.

[19] E.D. Glendening, C.R. Landis, F. Weinhold, Nbo Version 3.1 Program Manual, Tci, Univ. Wisconsin, Madison,. (1998). https://Www.Ccl.Net/Cca/Software/Ms-Win95-Nt/Mopac6/Nbo.Htm.

[20] T.A. Keith, Aimall (Version 10.05. 04, Professional), Tk Gristmill Softw. Overl. Park. Ks, Usa. (1997).

[21] G. Nichols, C.S. Frampton, Physicochemical Characterization Of The Orthorhombic Polymorph Of Paracetamol Crystallized From Solution, J. Pharm. Sci. 87 (1998) 684–693. https://doi.org/10.1021/Js970483d.

[22] C. Castellari, S. Ottani, Two Monoclinic Forms Of Diclofenac Acid, Urn:Issn:0108-2701. 53 (1997) 794–797. https://doi.org/10.1107/S0108270197002126.

[23] A.. G. Orpen, L. Brammer, F.H. Allen, O. Kennard, D.G. Watson, R. Taylor, Appendix A: Typical Interatomic Distances In Organic Compounds And Organometallic Compounds And Coordination Complexes Of The D- And F-Block Metals, Struct. Correl. (1994) 752–858. https://doi.org/10.1002/9783527616091.App1.

[24] H. Bougherara, R. Kadri, M. Kadri, M. Yekhlef, A. Boumaza, Complex Of 4-(2-Aminophenyl) −1,2,3- Thiadiazole With 2,3-Dichloro- 5,6-Dicyano-1,4-Benzoquinone: Experimental Study And Investigation At Different Exchange-Correlation Functionals. Dos, Nbo, Qtaim And Rdg Analyses, J. Mol. Struct. 1223 (2021) 128855. https://doi.org/10.1016/J.Molstruc.2020.128855.

[25] J. Uma Maheswari, S. Muthu, T. Sundius, Qm/Mm Methodology, Docking And Spectroscopic (Ft-Ir/Ft-Raman, Nmr, Uv) And Fukui Function Analysis On Adrenergic Agonist, Spectrochim. Acta Part A Mol. Biomol. Spectrosc. 137 (2015) 841–855. https://doi.org/10.1016/J.Saa.2014.07.095.

[26] Y. Danten, T. Tassaing, M. Besnard, Density Functional Theory (Dft) Calculations Of The Infrared Absorption Spectra Of Acetaminophen Complexes Formed With Ethanol And Acetone Species, 110 (2006) 8986. https://doi.org/10.1021/Jp061845l.

[27] C. Arunagiri, M. Arivazhagan, A. Subashini, Vibrational Spectroscopic (Ft-Ir And Ft-Raman), First-Order Hyperpolarizablity, Homo, Lumo, Nbo, Mulliken Charges And Structure Determination Of 2-Bromo-4-Chlorotoluene, Spectrochim. Acta Part A Mol. Biomol. Spectrosc. 79 (2011) 1747–1756. https://doi.org/10.1016/J.Saa.2011.05.050.

[28] T.O. Hodson, Root-Mean-Square Error (Rmse) Or Mean Absolute Error (Mae): When To Use Them Or Not, Geosci. Model Dev. 15 (2022) 5481–5487. https://doi.org/10.5194/Gmd-15-5481-2022.

[29] I.G. Binev, P. Vassileva-Boyadjieva, Y.I. Binev, Experimental And Ab Initio Mo Studies On The Ir Spectra And Structure Of 4-Hydroxyacetanilide (Paracetamol), Its Oxyanion And Dianion, J. Mol. Struct. 447 (1998) 235–246. https://doi.org/10.1016/S0022-2860(98)00302-0.

[30] T.N. Drebushchak, E. V. Boldyreva, Variable Temperature (100-360 K) Single-Crystal X-Ray Diffraction Study Of The Orthorhombic Polymorph Of Paracetamol (P-Hydroxyacetanilide), Zeitschrift Fur Krist. 219 (2004) 506–512. https://doi.org/10.1524/Zkri.219.8.506.38329.

[31] A.O. Surov, I. V. Terekhova, A. Bauer-Brandl, G.L. Perlovich, Thermodynamic And Structural Aspects Of Some Fenamate Molecular Crystals, Cryst. Growth Des. 9 (2009) 3265–3272. Https://doi.org/10.1021/Cg900002q.

[32] P. Gund, T.Y. Shen, A Model For The Prostaglandin Synthetase Cyclooxygenation Site And Its Inhibition By Antiinflammatory Arylacetic Acids, J. Med. Chem. 20 (1977) 1146–1152. https://doi.org/10.1021/Jm00219a007.

[33] Y. Wang, S. Saebø, C.U. Pittman, The Structure Of Aniline By Ab Initio Studies, J. Mol. Struct. Theochem. 281 (1993) 91–98. https://doi.org/10.1016/0166-1280(93)87064-K.

[34] M.A. Palafox, Dft Computations On Vibrational Spectra: Scaling Procedures To Improve The Wavenumbers, Phys. Sci. Rev. 3 (2019). https://doi.org/10.1515/Psr-2017-0184.

[35] M.H. Jamroz, Vibrational Energy Distribution Analysis (Veda): Scopes And Limitations, Spectrochim. Acta Part A Mol. Biomol. Spectrosc. 114 (2013) 220–230. https://doi.org/10.1016/J.Saa.2013.05.096.

[36] G. Varsányi, Assignments For Vibrational Spectra Of Seven Hundred Benzene Derivatives, John Wiley & Sons, 1974.

[37] G. Socrates, Infrared And Raman Characteristic Group Frequencies, 3rd Ed., Wiley Chichester, 2001.

[38] R.M. Silverstein, F.X. Webster, D.J. Kiemle., Spectrometric Identification Of Organic Compounds, 7th Ed., John Wiley & Sons. Inc, 2005.

[39] N.G.P. Roeges, A Guide To The Complete Interpretation Of The Infrared Spectra Of Organic Structures, 4th Ed., John Wiley & Sons. Inc, 1994.

[40] N.S. Sundar, C. Santhamma, Electronic Absorption Spectra Of 2-Amino-6-Nitro-, 4-Amino-3-Bromo-And 5-Amino-2-Bromotoluenes, Spectrochim. Acta Part A Mol. Spectrosc. 43 (1987) 1087–1098. https://doi.org/10.1016/0584-8539(87)80184-8.
[41] A.S. El-Shahawy, S.M. Ahmed, N.K. Sayed, Indo/Scf-Ci Calculations And Structural Spectroscopic Studies Of Some Complexes Of 4-Hydroxyacetanilide, 66 (2007) 143–152. https://doi.org/10.1016/J.Saa.2006.02.034.
[42] K. Raju, G. Gopkumar, G. Krishnakumar, H.T. Varghese, C.Y. Panicker, Vibrational Spectroscopic Studies And Dft Calculations Of 4-Hydroxyacetanilide, Mater. Sci. Res. India. 5 (2008) 75–82.
[43] P. Govindasamy, S. Gunasekaran, G.R. Ramkumaar, Natural Bond Orbital Analysis, Electronic Structure And Vibrational Spectral Analysis Of N-(4-Hydroxyl Phenyl) Acetamide: A Density Functional Theory, Spectrochim. Acta - Part A Mol. Biomol. Spectrosc. 130 (2014) 621–633. https://doi.org/10.1016/J.Saa.2014.03.065.
[44] K. Anitha, V. Balachandran, Assessment Of Long-Range Corrected And Conventional Dft Functional For The Prediction Of Second - Order Nlo Properties And Other Molecular Properties Of N-(2-Cyanoethyl)-N-Butylaniline - A Vibrational Spectroscopy Study, Spectrochim. Acta - Part A Mol. Biomol. Spectrosc. 146 (2015) 66–79. https://doi.org/10.1016/J.Saa.2015.03.048.
[45] J.S. Al-Otaibi, Vibrational (Ft-Ir And Ft-Raman) Spectroscopic Studies Using Ab Initio (Hf) And Dft (B3lyp) Calculations Of Paracetamol, Int. J. Biol. Pharm. Allied Sci.(Ijbpas). 5 (2016) 887–899.
[46] P. Govindasamy, S. Gunasekaran, Quantum Mechanical Calculations And Spectroscopic (Ft-Ir, Ft-Raman And Uv) Investigations, Molecular Orbital, Nlo, Nbo, Nlmo And Mesp Analysis Of 4-[5-(4-Methylphenyl)-3-(Trifluoromethyl)-1h-Pyrazol-1-Yl] Benzene-1-Sulfonamide, J. Mol. Struct. 1081 (2015). https://doi.org/10.1016/J.Molstruc.2014.10.011.
[47] K. Fukui, T. Yonezawa, C. Nagata, H. Shingu, Molecular Orbital Theory Of Orientation In Aromatic, Heteroaromatic, And Other Conjugated Molecules, J. Chem. Phys. 22 (2004) 1433. https://doi.org/10.1063/1.1740412.
[48] Y.S. Mary, Y.S. Mary, R. Thomas, B. Narayana, S. Samshuddin, B.K. Sarojini, S. Armaković, S.J. Armaković, G.G. Pillai, Theoretical Studies On The Structure And Various Physico-Chemical And Biological Properties Of A Terphenyl Derivative With Immense Anti-Protozoan Activity, Polycycl. Aromat. Compd. 41 (2021) 825–840. https://doi.org/10.1080/10406638.2019.1624974.
[49] Y.S. Kara, A. Esme, S. Sagdinc, Tdos/Pdos/Opdos, Reduced Density Gradient (Rdg) And Molecular Docking Studies Of [3-(3-Bromophenyl)-Cis-4,5-Dihydroisoxazole-4,5-Diyl]Bis(Methylene) Diacetate, J. Balıkesir Univ. Inst. Sci. Technol. 24 (2022) 100–110. https://doi.org/10.25092/Baunfbed.870307.
[50] S. Christopher Jeyaseelan, A. Milton Franklin Benial, K. Kaviyarasu, Vibrational, Spectroscopic, Chemical Reactivity, Molecular Docking And In Vitro Anticancer Activity Studies Against A549 Lung Cancer Cell Lines Of 5-Bromo-Indole-3-Carboxaldehyde, J. Mol. Recognit. 34 (2021). https://doi.org/10.1002/Jmr.2873.
[51] R.G. Pearson, Absolute Electronegativity And Hardness: Applications To Organic Chemistry, J. Org. Chem. 54 (1989) 1423–1430. https://doi.org/10.1021/Jo00267a034.
[52] T. Koopmans, Über Die Zuordnung Von Wellenfunktionen Und Eigenwerten Zu Den Einzelnen Elektronen Eines Atoms, Physica. 1 (1934) 104–113. https://doi.org/10.1016/S0031-8914(34)90011-2.
[53] H. Amzal, Quantum Chemistry Investigation Of Solvent Effect On The Ionization Potential Of Two Anti Inflammatory Molecules: Aspirin And Acetaminophen, Moroccan J. Heterocycl. Chem. 17 (2018). https://doi.org/10.48369/Imist.Prsm/Jmch-V17i2.14121.
[54] C.B. Aakeröy, T.K. Wijethunga, J. Desper, Molecular Electrostatic Potential Dependent Selectivity Of Hydrogen Bonding, New J. Chem. 39 (2015) 822–828. https://doi.org/10.1039/C4nj01324g.
[55] R.F.W. Bader, M.T. Carroll, J.R. Cheeseman, C. Chang, Properties Of Atoms In Molecules: Atomic Volumes, J. Am. Chem. Soc. 109 (1987) 7968–7979. https://doi.org/10.1021/Ja00260a006.
[56] P. Politzer, J.S. Murray, Z. Peralta-Inga, Molecular Surface Electrostatic Potentials In Relation To Noncovalent Interactions In Biological Systems, Int. J. Quantum Chem. 85 (2001) 676–684. https://doi.org/10.1002/Qua.1706.
[57] P. Moser, A. Sallmann, I. Wiesenberg, Synthesis And Quantitative Structure-Activity Relationships Of Diclofenac Analogues, J. Med. Chem. 33 (1990) 2358–2368. https://doi.org/10.1021/Jm00171a008.
[58] S. Ramalingam, M. Karabacak, S. Periandy, N. Puviarasan, D. Tanuja, Spectroscopic (Infrared, Raman, Uv And Nmr) Analysis, Gaussian Hybrid Computational Investigation (Mep Maps/Homo And Lumo) On Cyclohexanone Oxime, Spectrochim. Acta Part A Mol. Biomol. Spectrosc. 96 (2012) 207–220. https://doi.org/10.1016/J.Saa.2012.03.090.
[59] S. Sivaprakash, S. Prakash, S. Mohan, S.P. Jose, Molecular Structure, Vibrational Analysis (Ir And Raman) And Quantum Chemical Investigations Of 1-Aminoisoquinoline, J. Mol. Struct. 1149 (2017) 835–845. Https://doi.org/10.1016/J.Molstruc.2017.08.060.
[60] C.Y. Panicker, H.T. Varghese, K.C. Mariamma, K. John, S. Mathew, J. Vinsova, C. Van Alsenoy, Y.S. Mary, Spectroscopic Investigations And Computational Study Of 2-[Acetyl(4-Bromophenyl)Carbamoyl]-4-Chlorophenyl Acetate, J. Raman Spectrosc. 41 (2010) 707–716. https://doi.org/10.1002/Jrs.2492.
[61] N. Issaoui, H. Ghalla, F. Bardak, M. Karabacak, N. Aouled Dlala, H.T. Flakus, B. Oujia, Combined Experimental And Theoretical Studies On The Molecular Structures, Spectroscopy, And Inhibitor Activity Of 3-(2-Thienyl)Acrylic Acid Through Aim, Nbo,Ft-Ir, Ft-Raman, Uv And Homo-Lumo Analyses, And Molecular Docking, J. Mol. Struct. 1130 (2017) 659–668. https://doi.org/10.1016/J.Molstruc.2016.11.019.
[62] N.R. Sheela, S. Muthu, S. Sampathkrishnan, A.A. Al-Saadi, Normal Co-Ordinate Analysis, Molecular Structural, Non-Linear Optical, Second Order Perturbation Studies Of Tizanidine By Density Functional Theory, Spectrochim. Acta Part A Mol. Biomol. Spectrosc. 139 (2015) 189–199. https://doi.org/10.1016/J.Saa.2014.11.065.
[63] S.A. Siddiqui, T. Rasheed, M. Faisal, A.K. Pandey, S.B. Khan, Electronic Structure, Nonlinear Optical Properties, And Vibrational Analysis Of Gemifloxacin By Density Functional Theory, Spectrosc. (New York). 27 (2012) 185–206. https://doi.org/10.1155/2012/614710.
[64] B. Amul, S. Muthu, M. Raja, S. Sevvanthi, Spectral, Dft And Molecular Docking Investigations On Etodolac, J. Mol. Struct. 1195 (2019) 747–761. https://doi.org/10.1016/J.Molstruc2019.06.047.
[65] R. F. W. Bader, Atoms In Molecules: A Quantum Theory, Oxford University Press (Oup), 1990.
[66] B.R. Raajaraman, N.R. Sheela, S. Muthu, Investigation On 1-Acetyl-4-(4-Hydroxyphenyl) Piperazine An Anti-Fungal Drug By Spectroscopic, Quantum Chemical Computations And Molecular Docking Studies, J. Mol. Struct. 1173 (2018) 583–595. https://doi.org/10.1016/J.Molstruc.2018.07.030.
[67] U. Koch, P.L.A. Popelier, Characterization Of C-H-O Hydrogen Bonds On The Basis Of The Charge Density, J. Phys. Chem. 99 (1995) 9747–9754. https://doi.org/10.1021/J100024a016.
[68] E. Espinosa, I. Alkorta, J. Elguero, E. Molins, From Weak To Strong Interactions: A Comprehensive Analysis Of The Topological And Energetic Properties Of The Electron Density Distribution Involving X–H···F–Y Systems, J. Chem. Phys. 117 (2002) 5529–5542. https://doi.org/10.1063/1.1501133.
[70] L. Pallavi, J. Tonannavar, J. Tonannavar, Dft Zwitterion Model For Vibrational And Electronic Structure Of Unnatural 3-Amino-3-

(4-Fluorophenyl)Propionic Acid, Aided By Ir And Raman Spectroscopy, J. Mol. Struct. 1211 (2020) 128085. https://doi.org/10.1016/J.Molstruc.2020.128085.